ETH zürich

PAUL SCHERRER INSTITUT
PSI

Master Thesis

Towards a Particle-Core Model for Cyclotrons

Author:
Pirmin Berger

Supervisor:
Dr. Andreas Adelmann

December 4, 2014

Understanding the outer region (halo) of a bunched beam is important for high intensity beams to minimize losses and activation. Particle-core models separate the motion of halo particles from the core and treats them as test-particles. Therefore these models are computationally inexpensive w.r.t full PIC simulations and can to some extend be derived analytically which also helps to better understand the mechanism of halo formation. These models have been successfully applied to linacs (first by Gluckstern in 1994 [1]) for coasting round beams. In this thesis the model is first extended to ellipsoidal 3D bunched beams acceleration is added. To reduce the number of input parameters (eg. degree of mismatch), a second model is developed which also predicts the motion of the core. It treats halo particles and core particles (macro-particles) together and includes dispersion and full 3D motion with angular momentum $L \geq 0$. These two models are then applied to cyclotrons close to real machines and the influence of the parameters is studied. The formation of a halo can be observed in both models depending on the current and mismatch of the beam.

Contents

1 Introduction

Understanding of beam halos is important for high intensity machines like the PSI cyclotrons. They can limit the intensity (current) of the machine, because they can cause beam loss and activation of the beam-pipe or other structures at extraction. For a precise simulation of the halo, eg. particle-in-cell (PIC) simulations can be used, which work by calculating the space-charge field on a grid.

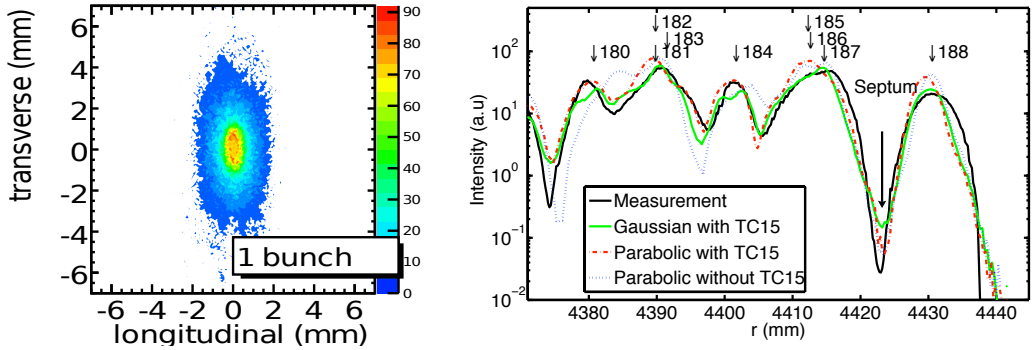

Figure 1.1: Beam bunch calculated with a PIC simulation, taken from [2] (left). Density at extraction, taken from [3] (right).

As these simulations are computationally expensive, reduced order models have been introduced for which the particle-core model is one of them. The first analytical particle-core model, on which this thesis will be based on, has been published in 1994 in a paper by Gluckstern [1]. It assumes a continuous, cylindrical KV (uniform density) beam which undergoes a breathing oscillation, which means that the radius $a(t)$ changes over time with

$$a(t) = a_0(1 - \varepsilon \cos(p \cdot t)) \tag{1.1}$$

for a small mismatch ε and core wave-number p. The focusing is constant, resulting in harmonic oscillations of test-particles with wave-number k in the absence of space-charge. The non-linear space-charge forces result in a amplitude dependent wave-number of test-particles which perform oscillations of the form

$$x(t) = \hat{x}(t) \cos(q \cdot t + \gamma(t)) \,, \tag{1.2}$$

with $\hat{x}(t)$ a slowly varying amplitude and $\gamma(t)$ the deviation from a harmonic oscillation. A parametric resonance effect between the core with wave-number p and

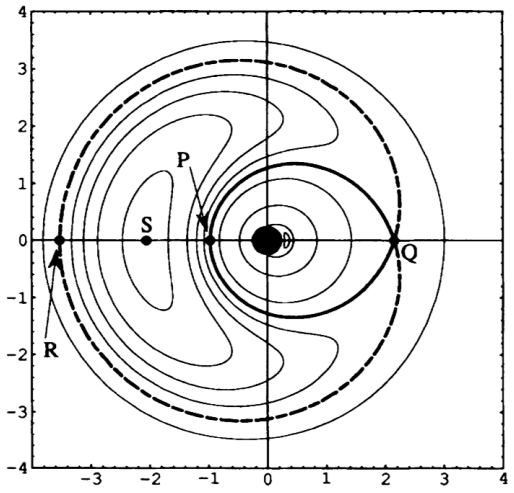

Figure 1.2: Contour plot of constant of motion of test-particles in phase-space. Plot taken from [1].

test-particles with wave-number q, eg. the 2:1 resonance with $2q = p$, can then influence the orbit of test-particles which can result in the formation of a halo.

Using some approximations, a constant of motion is derived from the equations of motion, which separates phase-space into 3 distinct regions shown in figure 1.2. The location of the (stable) fix-points and the critical points can now be used to estimate the properties of the beam halo. This model has already been extended in several directions, eg. for anisotropic (continuous) beams in circular accelerators by Ikegami et al. [4] or spherical bunches by Lund et al. [5]

The thesis consists of two parts. In the first part, the analytical particle-core model will be extended for accelerated ellipsoidal bunched beams and applied for different parameters. The second part introduces a new particle-core model, in which equations of motion for core and halo are solved numerically with fewer approximations, e.g. allowing for angular momentum > 0 and also including dispersion effects. This model is then applied to a simplified version of PSI Injector 2.

2 Analytical particle-core model

2.1 Separation of Core and Halo Particles

Particle core models were invented in the 90's (see eg. [1], [6], [7]) as a fast way of simulating non-linear space charge effect in particle beams. The full problem, in which each particle interacts with each other particle, is simplified by separating the bunch (or continuous beam) in two regions (see figure 2.1):

- *core*: contains most of the particles, collective description by eg. semi-axis, total charge etc.
- *halo*: particles outside of the core, single-particle description (x, p_x, y, ...)

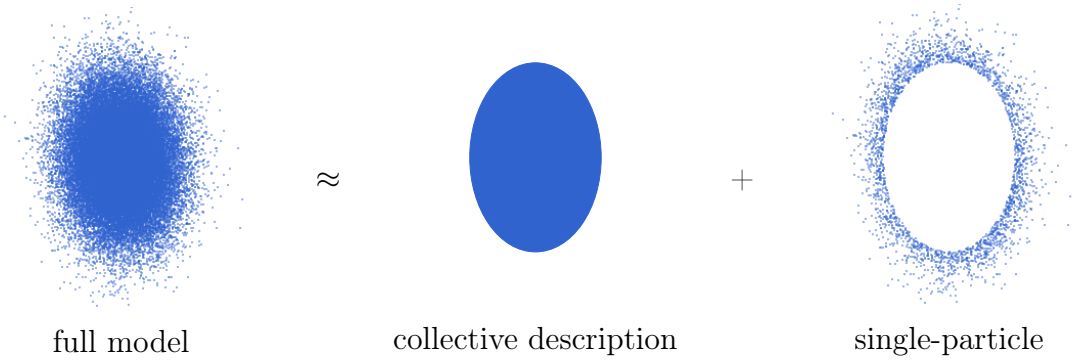

Figure 2.1: Separation of a bunch in core and halo particles

As the number of particles in the core is much higher than in the halo, halo particles are mostly influenced by the core and the influence of other halo particles is neglected as an approximation. Also, the influence of the halo particles on the core is small and therefore will be neglected too.

2.2 Coordinate System and Units

A Frenet-Serret coordinate system is used along the reference trajectory. It is oriented in a way, such that the reference particle is moving along positive z-direction and the x-direction points to the center of the cyclotron. To make the application of this model more convenient for isochronous cyclotrons, the time t, which can be easily related to the turn number n, is used as independent variable instead of the

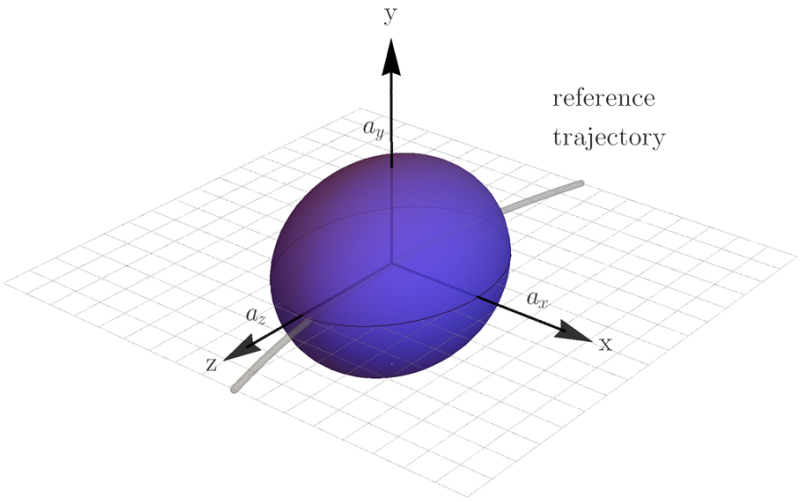

Figure 2.2: Coordinate system and bunch semi-axes, later referenced as *local frame*.

position along the reference trajectory s (as in the original model [1]).

Generalized perveance:

In physics of space charge effects, the dimensionless generalized perveance (first introduced by Lawson [8]) is commonly used. It is defined as

$$\kappa = \frac{2}{(\gamma\beta)^3}\frac{I_{\text{peak}}}{I_0} \tag{2.1}$$

with the Budker/Alfven current $I_0 = 4\pi\varepsilon_0\frac{mc^3}{e} \approx 3.12974 \cdot 10^7 A$ for protons. The mean current I of a bunched beam with bunch charge Q, revolution frequency f_{rev} and harmonic number h is given by

$$I = f_{\text{rev}} h Q = \tfrac{4}{3} f_{\text{rev}} h \pi a_x a_y a_z \rho\,. \tag{2.2}$$

To calculate the peak current, the ellipsoid near the center plane is approximated as cylinder with the same charge density ρ and cross-section and an infinitesimal length dl. With ρ given by Eq. (2.2), the peak current can be written as

$$I_{\text{peak}} = \frac{4}{3}\frac{I\beta c}{f_{\text{rev}} h a_z} \tag{2.3}$$

which can be plugged into (2.1) to yield

$$\kappa = \frac{3}{2}\frac{cI}{I_0\beta^2\gamma^3 f_{\text{rev}} h a_z} = \frac{3}{8\pi\varepsilon_0}\frac{q_e I}{\beta^2 c^2 \gamma^3 f_{\text{rev}} h a_z m_p}\,. \tag{2.4}$$

2.3 Potential of a Homogeneous Ellipsoidal Bunch

In the interior (denoted by subscript i) of a homogeneous ellipsoid with semi-axis a_x, a_y and a_z, and a total charge $Q = \frac{4}{3}\pi a_x a_y a_z \rho$ the electrostatic potential is a quadratic functional of x, y and z [9]:

$$U_i = \frac{Q}{4\pi\epsilon_0} \int_0^\infty \frac{1}{\sqrt{\phi(s)}} \left(1 - \frac{x^2}{a_x^2+s} - \frac{y^2}{a_y^2+s} - \frac{z^2}{a_z^2+s}\right) \mathrm{d}s \tag{2.5}$$

with $\phi(s) = (a_x^2+s)(a_y^2+s)(a_z^2+s)$. Using the modern definition of the Carlson symmetric forms

$$R_F(x,y,z) = \tfrac{1}{2} \int_0^\infty \frac{\mathrm{d}t}{\sqrt{(t+x)(t+y)(t+z)}}\,, \tag{2.6}$$

$$R_D(x,y,z) = \tfrac{3}{2} \int_0^\infty \frac{\mathrm{d}t}{(t+z)\sqrt{(t+x)(t+y)(t+z)}} \tag{2.7}$$

which are suited for fast and robust computation, the elliptic integral can be rewritten to

$$U_i = \frac{Q}{4\pi\epsilon_0}\frac{1}{2}\Bigg(3R_F(a_x^2,a_y^2,a_z^2) - x^2 R_D(a_y^2,a_z^2,a_x^2) - y^2 R_D(a_z^2,a_x^2,a_y^2) - z^2 R_D(a_x^2,a_y^2,a_z^2)\Bigg) \tag{2.8}$$

which reduces to

$$U_i = \frac{Q}{4\pi\epsilon_0}\frac{1}{2a}\left(3 - \frac{r^2}{a^2}\right) \tag{2.9}$$

in the case of a spherical bunch with radius a. In the exterior region (denoted by subscript e) of the ellipsoid, the potential is given by [9]

$$U_e = \frac{Q}{4\pi\epsilon_0} \int_\lambda^\infty \frac{1}{\sqrt{\phi(s)}} \left(1 - \frac{x^2}{a_x^2+s} - \frac{y^2}{a_y^2+s} - \frac{z^2}{a_z^2+s}\right) \mathrm{d}s \tag{2.10}$$

with λ the largest root of the equation

$$\frac{x^2}{a_x^2+\lambda} + \frac{y^2}{a_y^2+\lambda} + \frac{z^2}{a_z^2+\lambda} - 1 = 0\,. \tag{2.11}$$

Using a change of variables $s \to s' = s - \lambda$ this integral can also be reduced to a sum of Carlson symmetric forms:

$$U_e = \frac{Q}{4\pi\epsilon_0}\frac{1}{2}\Bigg(3R_F(a_x^2+\lambda, a_y^2+\lambda, a_z^2+\lambda)$$
$$-x^2 R_D(a_y^2+\lambda, a_z^2+\lambda, a_x^2+\lambda) - y^2 R_D(a_z^2+\lambda, a_x^2+\lambda, a_y^2+\lambda) - z^2 R_D(a_x^2+\lambda, a_y^2+\lambda, a_z^2+\lambda)\Bigg). \tag{2.12}$$

In the special case for a particle on the x-axis, $\lambda = x^2 - a_x^2$ can be substituted. Applying then the symmetry properties of the integrals, this leads to

$$U_e(x, y=0, z=0) = \frac{Q}{4\pi\epsilon_0}\frac{1}{2}\Bigg(3R_F(x^2+a_y^2-a_x^2, x^2+a_z^2-a_x^2, x^2) - x^2 R_D(x^2+a_y^2-a_x^2, x^2+a_z^2-a_x^2, x^2)\Bigg). \tag{2.13}$$

The pre-factor $\frac{Q}{4\pi\epsilon_0}$ can be expressed through the unitless quantity κ by

$$\frac{Q}{4\pi\epsilon_0} = \frac{2\kappa\beta^2 c^2\gamma^3 a_z m_p}{3q_e}. \tag{2.14}$$

2.4 Small-Mismatch Core Envelope Evolution

To describe the evolution of the core, the set of three coupled envelope equations for bunched beams can be used. Assuming a small mismatch, it has been shown that three modes are present: a pure transverse quadrupolar mode (subscript q) and a high (subscript h) and low (subscript l) mode in which transverse and longitudinal directions are coupled [10]. The tunes of these modes are

$$\begin{aligned}
\sigma_{\text{env,q}} &= 2\sigma_t \\
\sigma_{\text{env,h}} &= \sqrt{A+B} \\
\sigma_{\text{env,l}} &= \sqrt{A-B} \\
A &= \sigma_{t0}^2 + \sigma_t^2 + \tfrac{1}{2}\sigma_{l0}^2 + \tfrac{3}{2}\sigma_l^2 \\
B &= \sqrt{(\sigma_{t0}^2 + \sigma_t^2 - \tfrac{1}{2}\sigma_{l0}^2 - \tfrac{3}{2}\sigma_l^2)^2 + (\sigma_{t0}^2 - \sigma_t^2)(\sigma_{l0}^2 - \sigma_l^2)}
\end{aligned} \tag{2.15}$$

with the full and zero current transverse and longitudinal tunes σ_t, σ_{t0}, σ_l and σ_{l0}.

The motion of the core is then given by

$$\begin{aligned}
a_x(t) &= a_x \cdot (1 + C_{hr}\cos(p_h t) + C_{lr}\cos(p_l t) + C_{qr}\cos(p_q t)) \\
a_y(t) &= a_y \cdot (1 + C_{hv}\cos(p_h t) + C_{lv}\cos(p_l t) - C_{qv}\cos(p_q t)) \\
a_z(t) &= a_z \cdot (1 + C_{hl}\cos(p_h t) - C_{ll}\cos(p_l t))
\end{aligned} \tag{2.16}$$

where the C_{ij} coefficients denote the *mismatch coefficients* and p_q, p_h and p_l are the wave numbers of the three modes. The high-mode corresponds to a breathing oscillation whereas in the low-mode the longitudinal oscillation has opposite phase of the transverse oscillations.

2.5 Equation of Motion for Test-Particles (Halo)

The halo particles are described as single test-particles inside the field of the time-varying core. Assuming a constant focusing constant k_x and no dispersion, the equation of motion is

$$x''(t) + k_x^2 x(t) = \frac{q_e}{m_p} \cdot \vec{E}_{\mathrm{sc,x}}(x(t), y(t), z(t), t) \tag{2.17}$$

and analogous for y(t), z(t) with $\vec{E}_{\mathrm{sc}} = -\vec{\nabla} Q$. The space charge introduces a coupling between the directions.

To simplify the equation, the motion is first restricted to particles with zero angular momentum starting on the x-axis. Due to symmetry, their motion will stay confined on the x-axis and the equation of motion is

$$x''(t) + k_x^2 x(t) = \frac{q_e}{m_p} \cdot E_{\mathrm{sc,x}}(x(t), t) \tag{2.18}$$

which is an inhomogeneous second order ODE.

2.5.1 Tune Depression

Assume a *static* E-field due to the space charge of the ellipsoidal bunch. The equation of motion for particles inside of the core can be re-written as

$$\begin{aligned} x''(t) + k_{x,\mathrm{sc}}^2 x(t) &= 0 \\ k_{x,\mathrm{sc}}^2 &= k_x^2 - \tfrac{2}{3}\beta^2 c^2 \gamma^3 a_z \kappa R_D(a_y^2, a_z^2, a_x^2) \end{aligned} \tag{2.19}$$

with the new depressed focusing constant $k_{x,\mathrm{sc}}$ or equivalently the depressed tune $\nu_{x,\mathrm{sc}} = \frac{k_{x,\mathrm{sc}}}{\omega_c}$.

2.5.2 Taylor Expansions

To solve eq. (2.18) we plug in the electric field obtained by the potential given in eq. (2.8) and (2.13), inside and outside the bunch respectively.

The integrands in the Carlson elliptic integrals can be replaced by their Taylor Series around the mean value of their arguments [11] to yield

$$
\begin{aligned}
R_F(x,y,z) &\approx \frac{1}{\sqrt{A}}(1-\frac{1}{10}E_2)\\
A &= \frac{x+y+z}{3}\\
E2 &= \Delta x\Delta y+\Delta y\Delta z+\Delta z\Delta x\\
\Delta x &= 1-\frac{x}{A} \quad \text{and analogous for y and z}
\end{aligned}
\tag{2.20}
$$

and

$$
\begin{aligned}
R_D(x,y,z) &\approx A^{-\frac{3}{2}}(1-\frac{3}{14}E_2)\\
A &= \frac{x+y+3z}{5}\\
E2 &= \Delta x\Delta y+3\Delta x\Delta z+3\Delta y\Delta z+3(\Delta z)^2\\
\Delta x &= 1-\frac{x}{A} \quad \text{and analogous for y and z}
\end{aligned}
\tag{2.21}
$$

The semi-axes a_i of the bunch are then replaced by the time-varying expression given in eq. (2.16). As the mismatch coefficients C_{mn} in eq. (2.16) are small, the resulting expression is Taylor expanded to first order in all mismatch coefficients.

As the bunch is no too elongated in one direction, new variables $e=\sqrt{\frac{a_z^2-a_x^2}{a_z^2}}$ and $f=\sqrt{\frac{a_z^2-a_y^2}{a_z^2}}$ are introduced to replace a_x and a_y. The variables e and f are now small and the expression can be Taylor expanded to arbitrary order in them.

Similar to eq. (2.19), for particles inside the core, all terms linear in x(t) without explicit time dependence on the RHS are moved to the left and a new depressed focusing constant q is defined, including these terms. Finally, the equation of motion for test-particles inside the core can be written as

$$
x''(t)+q^2x(t)=\frac{\beta^2c^2\gamma^3\kappa}{a_z^2}\left(\tilde{C}_{\mathrm{ih}}\cos(p_ht)+\tilde{C}_{\mathrm{il}}\cos(p_lt)+\tilde{C}_{\mathrm{iq}}\cos(p_qt)\right)x(t) \tag{2.22}
$$

with new coefficients $\tilde{C}$, which depend on the mismatch coefficients C and e and f, and are for second order in e and f given by

$$
\begin{aligned}
\tilde{C}_{\mathrm{ih}} &= C_{\mathrm{hl}}\left(-\tfrac{3e^2}{7}-\tfrac{f^2}{7}-\tfrac{2}{5}\right)+C_{\mathrm{hr}}\left(-\tfrac{33e^2}{35}-\tfrac{3f^2}{7}-\tfrac{6}{5}\right)+C_{\mathrm{hv}}\left(-\tfrac{3e^2}{7}-\tfrac{f^2}{35}-\tfrac{2}{5}\right)\\
\tilde{C}_{\mathrm{il}} &= C_{\mathrm{ll}}\left(\tfrac{3e^2}{7}+\tfrac{f^2}{7}+\tfrac{2}{5}\right)+C_{\mathrm{lr}}\left(-\tfrac{33e^2}{35}-\tfrac{3f^2}{7}-\tfrac{6}{5}\right)+C_{\mathrm{lv}}\left(-\tfrac{3e^2}{7}-\tfrac{f^2}{35}-\tfrac{2}{5}\right)\\
\tilde{C}_{\mathrm{iq}} &= C_{\mathrm{qr}}\left(-\tfrac{33e^2}{35}-\tfrac{3f^2}{7}-\tfrac{6}{5}\right)+C_{\mathrm{qv}}\left(\tfrac{3e^2}{7}+\tfrac{f^2}{35}+\tfrac{2}{5}\right)\\
q^2 &= k^2-\tfrac{\beta^2c^2\gamma^3\kappa}{a_z^2}\left(\tfrac{2}{3}+\tfrac{3}{5}e^2+\tfrac{1}{5}f^2\right).
\end{aligned}
\tag{2.23}
$$

Higher order formulas of these coefficients are given in the appendix. Eq. (2.22), which is only valid for particles inside the core and has the form of a **Mathieu equation**. Outside of the core, the equations is more complicated:

$$\begin{aligned} x''(t) + q^2 x(t) = &-\left(\tfrac{2}{3} + \tfrac{3}{5}e^2 + \tfrac{1}{5}f^2\right)\frac{\beta^2 c^2 \gamma^3 \kappa |x(t)|}{a_z^2} + \frac{2}{3}\frac{\beta^2 c^2 \gamma^3 \kappa |x(t)| a_z}{x^3(t)} \\ &\frac{\beta^2 c^2 \gamma^3 \kappa |x(t)| a_z^5}{x^7(t)} \sum_{i\in(h,l,q)} \tilde{C}_{\mathrm{o6},i} \cos(p_i t) + \frac{\beta^2 c^2 \gamma^3 \kappa |x(t)| a_z^3}{x^5(t)} \left(\tfrac{1}{5}f^2 - \tfrac{2}{5}e^2 + \sum_{i\in(h,l,q)} \tilde{C}_{\mathrm{o4},i} \cos(p_i t) \right) \end{aligned} \tag{2.24}$$

with coefficients

$$\begin{aligned} \tilde{C}_{\mathrm{o4,h}} &= -\tfrac{2}{5}(C_{hl} - 2C_{hr} + C_{hv}) - \tfrac{4}{5}C_{hr}e^2 + \tfrac{2}{5}C_{hv}f^2 \\ \tilde{C}_{\mathrm{o4,l}} &= \tfrac{2}{5}(C_{ll} + 2C_{lr} - C_{lv}) - \tfrac{4}{5}C_{lr}e^2 + \tfrac{2}{5}C_{lv}f^2 \\ \tilde{C}_{\mathrm{o4,q}} &= \tfrac{2}{5}(2C_{qr} + C_{qv}) - \tfrac{4}{5}C_{qr}e^2 - \tfrac{2}{5}C_{qv}f^2 \\ \tilde{C}_{\mathrm{o6,h}} &= \tfrac{4}{7}e^2(C_{hl} - 2C_{hr} + C_{hv}) + \tfrac{1}{7}f^2(-C_{hl} + 4C_{hr} - 3C_{hv}) \\ \tilde{C}_{\mathrm{o6,l}} &= \tfrac{1}{7}f^2(C_{ll} + 4C_{lr} - 3C_{lv}) - \tfrac{4}{7}e^2(C_{ll} + 2C_{lr} - C_{lv}) \\ \tilde{C}_{\mathrm{o6,q}} &= \tfrac{1}{7}f^2(4C_{qr} + 3C_{qv}) - \tfrac{4}{7}e^2(2C_{qr} + C_{qv}) \end{aligned} \tag{2.25}$$

2.5.3 Change of variables

Analogously to [1], a new scaled and squared variable $s(t)$ is introduced and is defined by

$$s(t) = \frac{x^2(t)}{a_x^2} = \frac{x^2(t)}{a_z^2(1-e^2)} \tag{2.26}$$

which transforms the equation of motion into

$$\begin{aligned} s''(t) - \frac{s'(t)^2}{2s(t)} + 2q^2 s(t) = \\ \frac{2\beta^2 c^2 \gamma^3 \kappa}{a_z^2} \begin{cases} \sum_{j\in(h,l,q)} \tilde{C}_{\mathrm{i},j} \cos(p_j t) & \text{if } s \le 1 \\ \frac{\sum_{j\in(h,l,q)} \tilde{C}_{\mathrm{o6},j} \cos(p_j t)}{(1-e^2)^{7/2} s(t)^{5/2}} + \frac{\sum_{j\in(h,l,q)} \tilde{C}_{\mathrm{o4},j} \cos(p_j t)}{(1-e^2)^{5/2} s(t)^{3/2}} + s(t)\left(\frac{2}{3} + \frac{3}{5}e^2 + \frac{1}{5}f^2\right) + & \text{if } s > 1 \\ \quad \frac{2}{3(1-e^2)^{3/2}\sqrt{s(t)}}\,. \end{cases} \end{aligned} \tag{2.27}$$

Since the equation of motion can be regarded as a harmonic oscillator with a small perturbation, the solution is expected to be approximately a harmonic oscillation, possibly with slowly varying amplitude. Therefore, $s(t)$ can be parametrized with the following ansatz

$$s(t) = \tfrac{1}{2}w(t)\big(1 - \cos(2qt + \gamma(t))\big)\,. \tag{2.28}$$

The ansatz eq. (2.28) can now be plugged into eq. (2.27) to yield an equation with two unknowns $w'(t)$ and $\gamma'(t)$. The assumption that is made now to simplify eq. (2.27) is, that $w(t)$ and $\gamma(t)$ are *slowly varying* with respect to t, in other words the time derivative of $s(t)$ with w and γ explicitly dependent on t must be equal the time derivative of $s(t)$ with w and γ assumed constant

$$\frac{d}{dt}\left(\tfrac{1}{2}w(t)\big(1 - \cos(2qt + \gamma(t))\big)\right) = \frac{d}{dt}\left(\tfrac{1}{2}w\big(1 - \cos(2qt + \gamma)\big)\right), \tag{2.29}$$

which leads to the condition

$$\gamma'(t) + \frac{w'(t)}{w(t)}\tan\left(\frac{2qt + \gamma(t)}{2}\right) = 0\,, \tag{2.30}$$

which is the second equation relating the two unknowns $w'(t)$ and $\gamma'(t)$ and therefore the system can be solved for these quantities.

2.5.4 Averaging over Fast Oscillations

As for the analysis of halo evolution the slowly varying amplitude of the particle motion is of more importance than the exact behavior of the fast oscillation, the obtained equations for $w'(t)$ and $\gamma'(t)$ are averaged over one period of the fast oscillation, for which we can assume w and γ constant. In this averaging procedure, one has to leave out the resonant terms with wave-number $2q - p$, which correspond to the 2:1 resonance [1]. Also, for $w > 1$ one has to consider, that the particle can leave or enter the core within one period. For convenience the total phase ψ of the oscillation will be used for averaging instead of the time. It consists of the harmonic oscillation phase ($2qt$) and a deviation from it ($\gamma(t)$) and is given by $\psi(t) = 2qt + \gamma(t)$. The phases ψ_1 and ψ_2 at which the test-particle leaves respectively enters the core can be obtained from Eq. (2.28) to $\psi_1 = \arccos(1 - \frac{2}{w})$ and $\psi_2 = 2\pi - \psi_1$ (remember $w(t) = w = \text{const}$ for one period). The averaging can then be expressed as

$$\overline{w}' = \tfrac{1}{2\pi}\left(\int_{-\psi_1}^{\psi_1} w'_{\text{inside}}\,\mathrm{d}\psi + \int_{\psi_1}^{2\pi-\psi_1} w'_{\text{outside}}\,\mathrm{d}\psi\right) \tag{2.31}$$

and equivalently for $\overline{\psi}'$. After averaging (omitting the overline from now on) one arrives at the coupled system of ODEs

$$\begin{aligned} w' &= \frac{\beta^2 c^2 \gamma^3 \kappa}{q a_z^2} \sum_{i\in(h,l,q)} \sin(\psi(t) - p_i t)\widetilde{W}_i(w(t)) \\ \psi' &= 2q + \frac{\beta^2 c^2 \gamma^3 \kappa}{q a_z^2}\Big(\widetilde{P}_0(w(t)) + \sum_{i\in(h,l,q)} \cos(\psi(t) - p_i t)\widetilde{P}_i(w(t))\Big) \end{aligned} \tag{2.32}$$

where some auxiliary functions $\widetilde{W_i}$ and $\widetilde{P_i}$ have been introduced to simplify notation. For example the contribution coming from the high-mode reads

$$\widetilde{W_{\mathrm{h}}}(w) = \begin{cases} \frac{\tilde{C}_{\mathrm{i,h}} w}{2} & \text{if } w \leq 1 \\ \frac{\tilde{C}_{\mathrm{o4,h}}\left(4\sqrt{w-1}\sqrt{w}-4\sinh^{-1}\left(\sqrt{w-1}\right)\right)}{\pi(1-e^2)^{5/2}w^{3/2}} - \frac{\tilde{C}_{\mathrm{o6,h}}\left(\sqrt{(w-1)w}(1-2w)+\sinh^{-1}\left(\sqrt{w-1}\right)\right)}{\pi(1-e^2)^{7/2}w^{5/2}} & \text{if } w > 1 \\ \quad + \frac{\tilde{C}_{\mathrm{i,h}}\left(w^2\left(\pi-2\tan^{-1}\left(\sqrt{w-1}\right)\right)-2\sqrt{w-1}w+4\sqrt{w-1}\right)}{2\pi w}. & \end{cases} \tag{2.33}$$

The definitions of the $\tilde{C}$ coefficients, the other auxiliary functions and higher orders are given in appendix A.

2.6 Constants of motion

For the special case of only one mode excited (eg. the low-mode), the system of equations (2.32) can be re-written using the definition $\Psi(t) = \psi(t) - p_h t$ as

$$\begin{aligned} w' &= \frac{\beta^2 c^2 \gamma^3 \kappa}{q a_z^2} \sin(\Psi) \tilde{W}_l(w) \\ \Psi' &= 2q - p_l + \frac{\beta^2 c^2 \gamma^3 \kappa}{q a_z^2} \left(\tilde{P}_0(w) + cos(\Psi) \tilde{P}_l(w) \right). \end{aligned} \tag{2.34}$$

For this system it is possible to find a constant of motion, corresponding to an autonomous Hamiltonian H, for which the system (2.34) is exactly Hamiltons equations ($\Psi' = \frac{\partial H}{\partial w}, w' = -\frac{\partial H}{\partial \Psi}$) for the pair of canonical variables (Ψ, w). Integrating the system (2.34), together with the observation that $\tilde{W}_l'(w) = \tilde{P}_l(w)$, H can be written as

$$H = (2q - p_l)w + \frac{\beta^2 c^2 \gamma^3 \kappa}{q a_z^2} \left(\cos(\Psi) \tilde{W}_l(w) + \int \tilde{P}_0(w) \mathrm{d}w \right) \tag{2.35}$$

where the indefinite integral of $\tilde{P}_0(w)$ can be computed analytically

$$\int \tilde{P}_0(w)\mathrm{d}w = \begin{cases} C_0 = \frac{-96e^2+8f^2+80}{30(1-e^2)^{5/2}} & \text{if } w \leq 1 \\ \frac{4\sinh^{-1}\left(\sqrt{w-1}\right)\left(20w(1-e^2)-2e^2+f^2\right)}{15\pi(1-e^2)^{5/2}w^{3/2}} + \frac{4\left(f^2-2e^2\right)\sqrt{w-1}}{15\pi(1-e^2)^{5/2}w} & \text{if } w > 1 \\ \quad + \frac{2\sqrt{w-1}\left(9e^2+3f^2+10\right)}{15\pi} + \frac{\left(-96e^2+8f^2+80\right)\sin^{-1}\left(\frac{1}{\sqrt{w}}\right)}{15\pi(1-e^2)^{5/2}} & \\ \quad + \frac{2(w-2)\left(9e^2+3f^2+10\right)\tan^{-1}\left(\sqrt{w-1}\right)}{15\pi}. & \end{cases} \tag{2.36}$$

Since H is a constant of motion, it can be used to characterize the trajectories of the halo particles. Plotting contours of constant H in w,Ψ phase-space results in similar plots than in [1].

The phase space visible in figure 2.3 consists of three different regions:

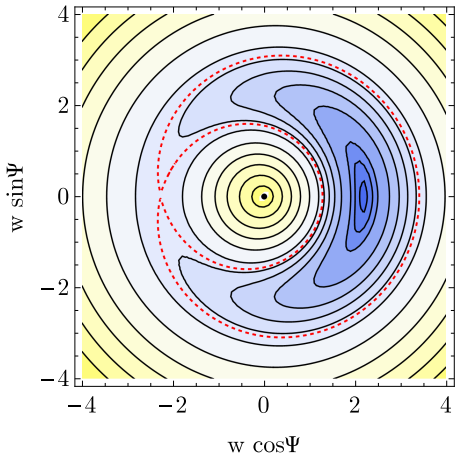

Figure 2.3: Contour plot of Hamiltonian for test-machine TEST1 (see table B.2), coasting beam, 50 turns, only high-mode excited with 5%

- core region: in the center of the core, both space-charge and focusing forces are small, the amplitude of particle motion only varies by small amount
- focusing dominated: for large w, the space charge forces ($\approx \frac{1}{r}$) become small compared to the focusing force ($\approx r$), the amplitude of particle motion also varies by only a small amount
- intermediate region: resonance with high oscillation amplitudes of the slowly varying amplitude. This resonance can bring particles from the region just outside the core to the outside of the outer separatrix

which are separated by 2 separatrices (red and dashed). For a static core, Ψ is a cyclic coordinate and therefore w is also a constant of motion.

For more than one mode excited, it is not possible to do the change of variables to conjugate coordinate pairs. Nevertheless, numerical simulation shows that there exists at least an approximate constant of motion. The time evolution of w in the case of the high and the low mode excited can be expressed as function of the phase differences $\Psi_h = \psi - p_h t$ and $\Psi_l = \psi - p_l t$ and plotted in toroidal coordinates with the angles Ψ_h and Ψ_l, the tube radius w and a large enough (eg. R=4) constant distance from the center to the tube center. For the inner (green) and outer (blue) region, the trajectories wind around approximate tori, whereas for the intermediate region (orange), the trajectories lie on a more complicated manifold. Figure 2.4 shows the lower half of these manifolds on the left-hand side and the phase-space of the one mode case for comparison on the right.

Figure 2.5 depicts the trajectories for and initial value of $\Psi_0 = 0$ which corresponds to zero transverse momentum or test-particle oscillation starting in phase with the core oscillation. The three types of trajectories are colored similar to the region in figure 2.4. In vicinity of the separatrices, the change in the amplitude of the

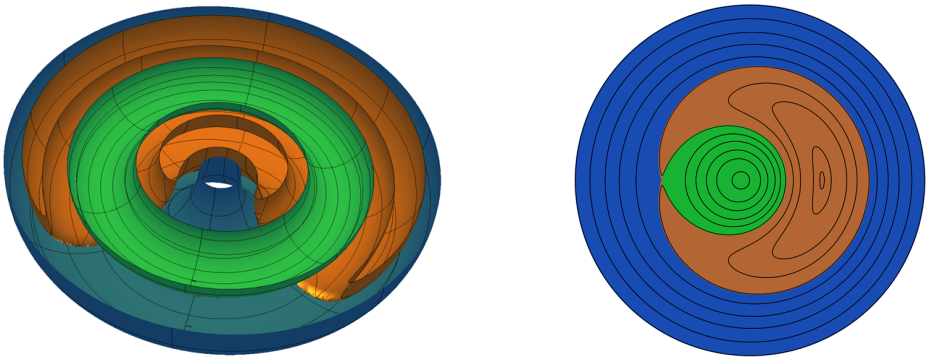

Figure 2.4: Lower half of three representative invariant manifolds of two mode case in toroidal coordinates (left) and phase-space of one mode case with invariants shown as black curves in polar coordinates (right). The phase-space regions on the right side are shown in similar colors than the corresponding representative manifolds on the left.

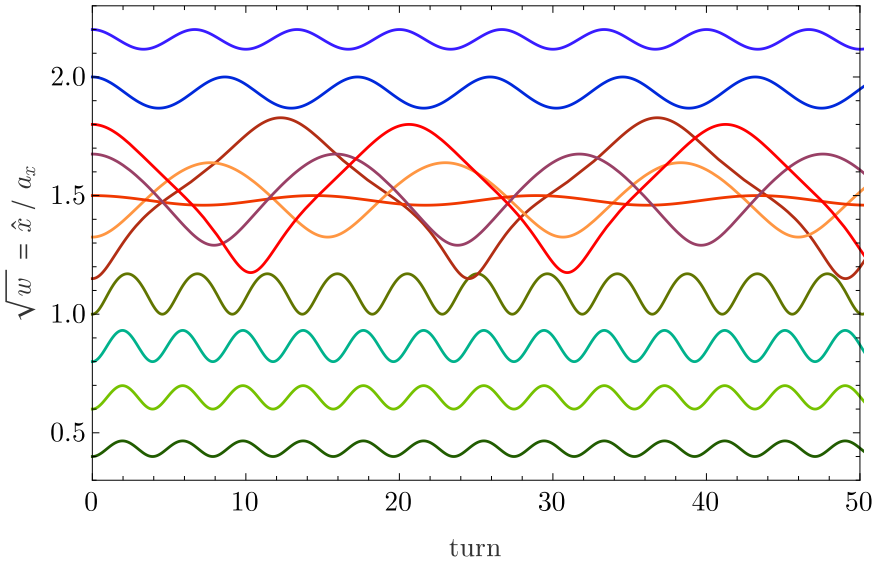

Figure 2.5: Trajectories for different initial values w_0 and $\Psi_0 = 0$, test-machine TEST1 (see table B.2), coasting beam, 50 turns, only high-mode excited with 5% (same parameters as in figure 2.3)

test-particles is relatively high (as can be already seen in figure 2.3) and the period of the oscillation of w is large. The time interval shown in figure 2.5 corresponds to approximately 50 turns in the test-machine (see table B.2), therefore the time-scale of the high amplitude oscillation with long periods is still short enough that it matters even for machines with few turns.

The figure 2.6 depicts the trajectories for same initial conditions of the test-

particles as in figure 2.5, but all 3 core modes excited.

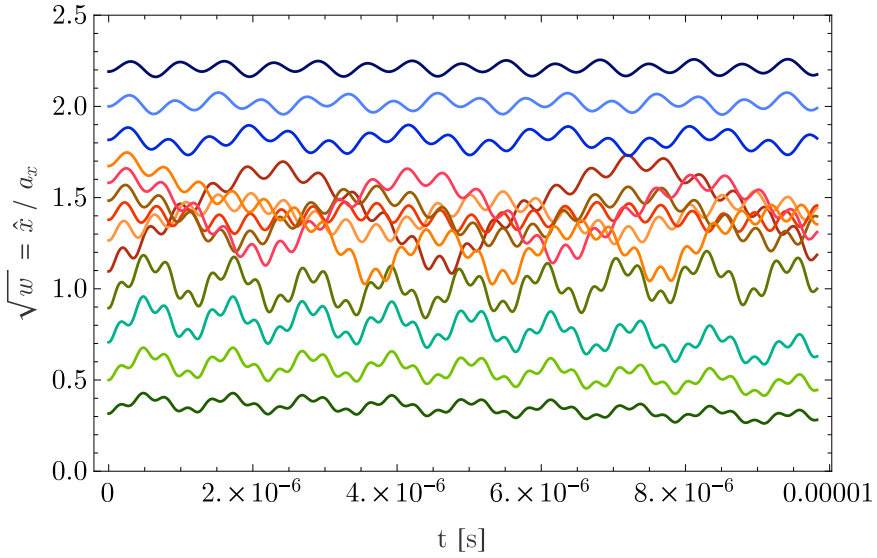

Figure 2.6: Trajectories for different initial values w_0 and $\Psi_0 = 0$, test-machine TEST2 (see table B.2), turn 5 coasting beam, all 3 modes excited

2.7 Influence of parameters

As a first step, the influence of the different input parameters on the phase-space is investigated by plotting the location of the unstable fix-point A, the stable fix-point C and the 2 critical points B and D, which correspond to the position of the separatrix for phase $\Psi = 0$. The position of the 4 points in phase-space is shown in figure 2.7.

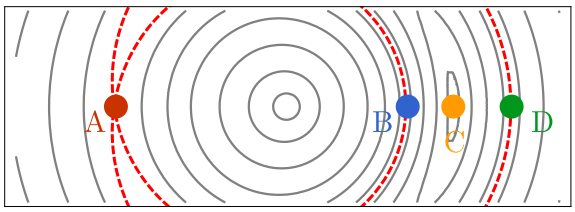

Figure 2.7: Naming convention of critical points and fix-points in w, Ψ phase-space.

Figure 2.8 shows the influence of the generalized perveance κ and the mismatch coefficients on the location of the fixed/critical points in the w, Ψ phase-space. Both, higher κ (e.g. through more current) and a higher mismatch lower the minimum distance of the separatrix (point B). For a lower position of this point, particles in the tails of the core are more likely to lie in the resonance region of the phase space

and end up in the halo. The maximum extend of the halo is characterized by the point D. It grows with higher mismatch, but goes down with higher κ. The width of the halo region seems to only depend on the mismatch and not on the space charge itself. For lower values of κ than in 2.8, the separatrices and therefore the resonance region in phase-space disappears.

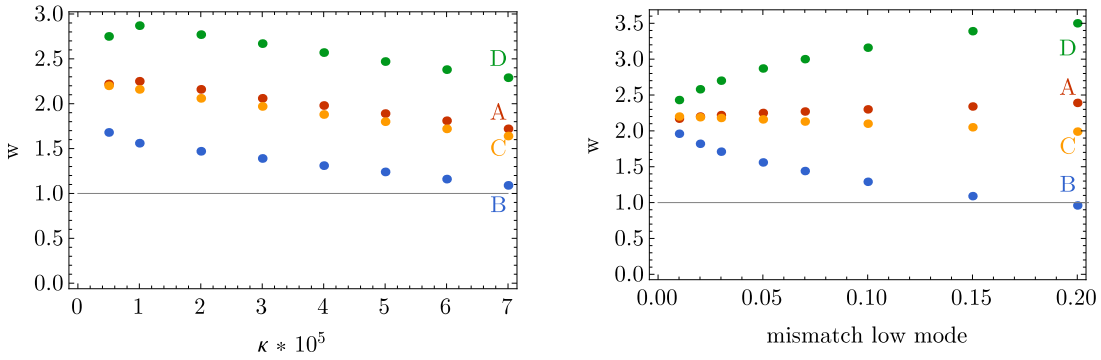

Figure 2.8: Location of stable/critical points for varying κ and fixed low mode mismatch of 0.05 (left), varying low mode mismatch and fixed κ of 10^{-5} (right).

For too high currents or a large mismatch, the location of the lower separatrix lies inside the core which makes the model inconsistent, because the core would (temporarily) loose particles to orbits with larger amplitudes, which would contradict the assumption that the total charge of the core remains constant. This imposes some limits on this model.

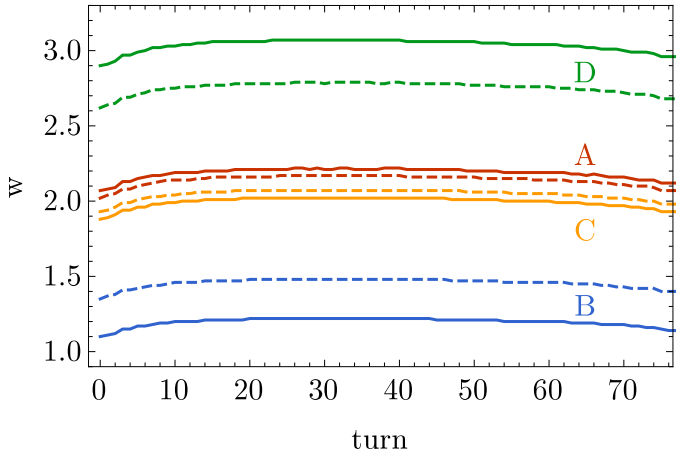

Figure 2.9: Location of critical/fix-points as function of turn number of test-machine TEST2. Dashed line is for lower mismatch coefficients.

2.8 Influence of averaging

One important step in the derivation of the analytical model is the averaging over the fast oscillations to arrive at equations (2.32). To verify this approximation, the averaged equations (2.32) are solved for the same initial conditions than the unaveraged equations (2.27). Figure 2.10 shows an example of the solutions of averaged and unaveraged equations.

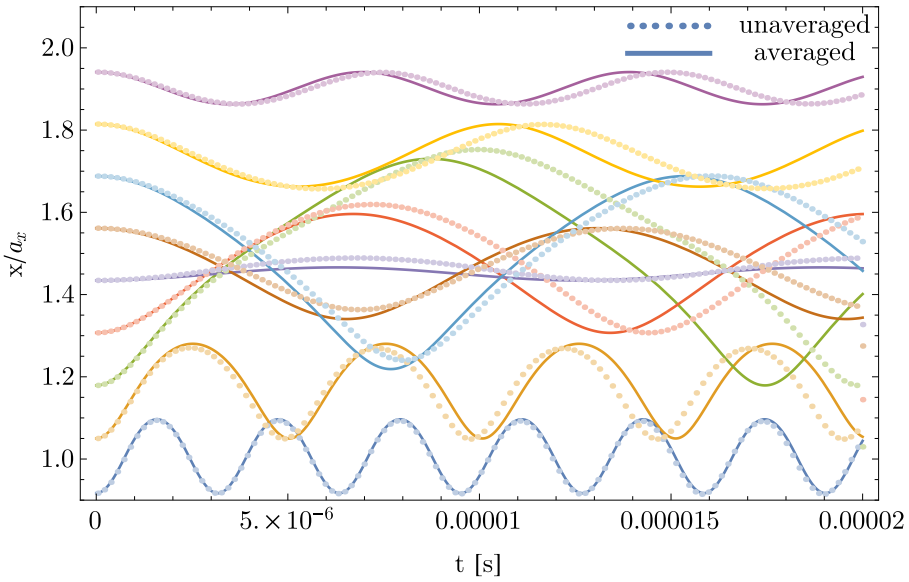

Figure 2.10: Slowly varying amplitudes in averaged (solid) and unaveraged (dotted) model.

In general the following can be observed:

- averaging has only little effect on the *amplitude* of w oscillations
- for $w \leq 1$ (particle always inside the core) the averaging is nearly exact
- for $w > 1$ the *frequency* of w oscillations differs up to the order of 10 %
- the error is largest near the separatrix (eg. green curve in figure 2.10)

It can be concluded that for applications where the exact time evolution is not important (eg. finding constants of motion and phase space regions), the approximation is valid to large extend, whereas for machines with varying parameters (eg. acceleration) the introduced error in time-scale can also have an influence on the amplitude of the particle oscillation if the parameters and therefore the location of the three phase-space regions change over time.

2.9 Tracking of distributions

Instead of tracking single particles only, whole distributions of test-particles can be tracked in x, p_x phase-space. At first, a coasting KV beam with Gaussian tails will be considered in a machine with similar parameters (tunes, energy, radius etc.) as PSI Injector 2 at turn 40. The mismatch is set to 10 % in the high mode ($C_{\mathrm{hr}} = C_{\mathrm{hv}} = C_{\mathrm{hl}} = 0.1$). Figure 2.11 depicts this initial distribution and how it evolved after 5, 27 and 78 turns. After a few turns spiral-like arms appear in the phase-space, which can be explained by the amplitude dependent wave-number for particles which are not always inside the core. This leads to different angular velocities in x, p_x phase-space and forms the spirals. After many turns the distribution (which looks like in the the bottom-right side of figure 2.11) stays stable and only performs a rotation in phase-space. The resonant region and its stable and unstable fix-points can be clearly seen in phase-space.

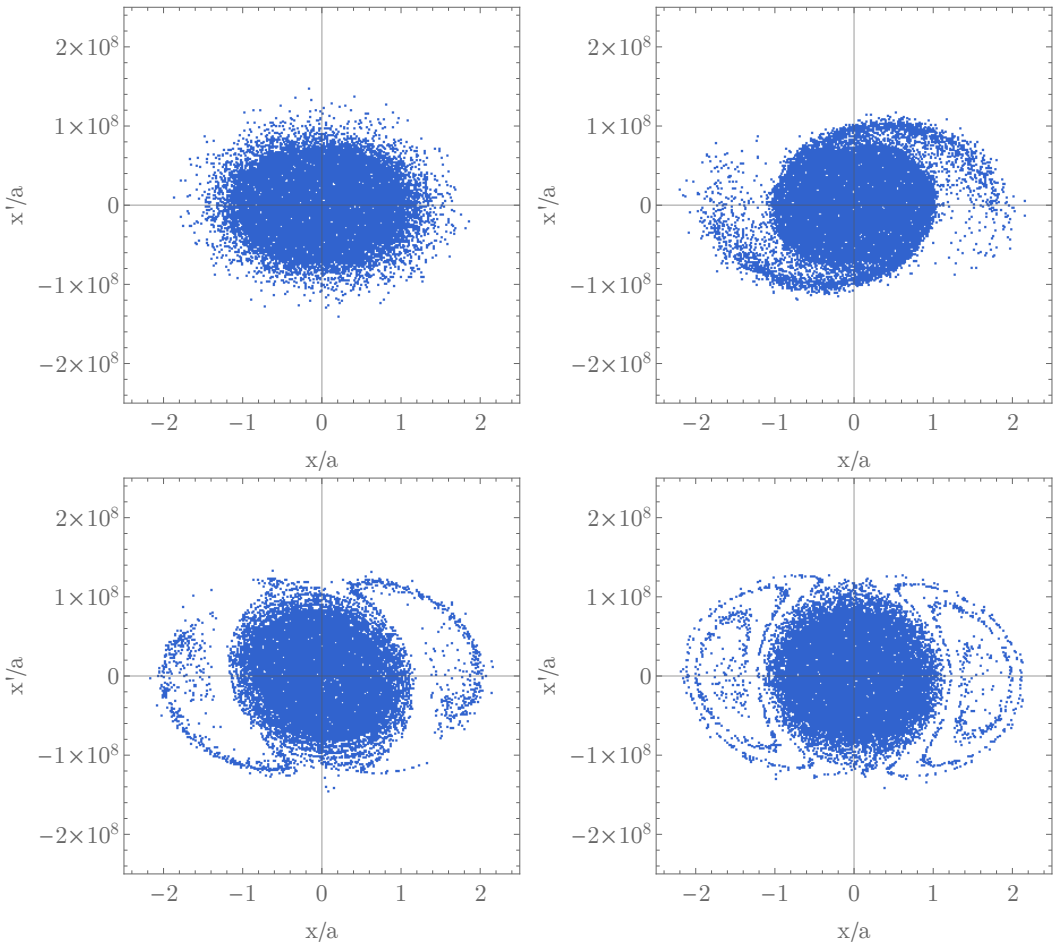

Figure 2.11: Phase space of TEST1 (Injector 2 like machine, coasting beam at 30 MeV). Initial distribution (top-left), after 5 (top-right), 27 (bottom-left) and 78 (bottom-right) turns for 10% excitation of high mode.

The same analysis can be done for a machine with acceleration. As the model does not refer to the fields of magnets and cavities directly, the influence of acceleration only enters via the change of parameters. The change in γ (relativistic gamma factor) affects the model in two ways: one one hand, the generalized perveance (Eq. (2.4)) is explicitly dependent on γ, a higher γ lowers the effect of space-charge. On the other hand other machine parameters like the tunes depend on radius which depends on the energy of the particle. Both effects have an influence on the location of the separatrices and the fix-points in phase-space. The consequence can be that if eg. the location of the outer separatrix gets closer to the center, particles just below the separarix can be above it after the parameters have changed. These particles are then in the outer region of the phase-space and perform oscillations with approximately constant high amplitude.

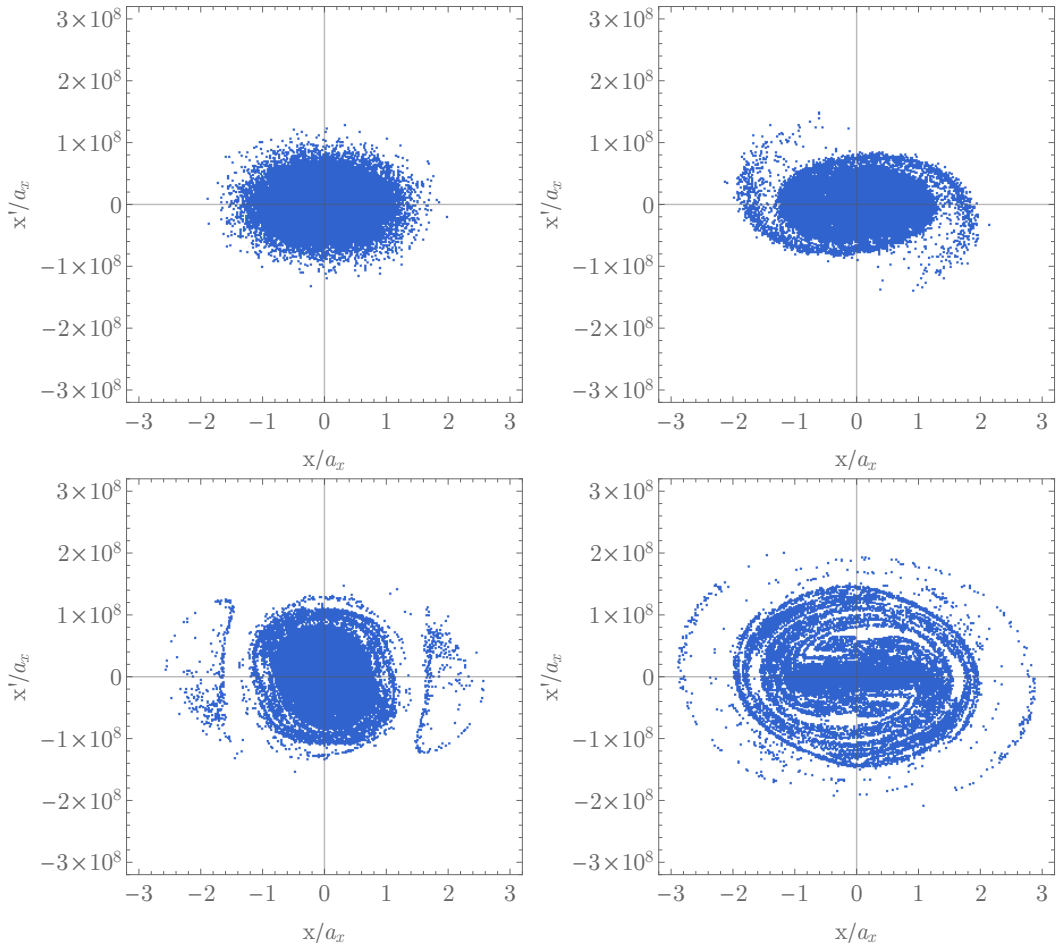

Figure 2.12: Phase space of TEST2 (accelerated beam Injector 2 like machine) after 0, 5, 27 and 78 turns for 10% excitation of high mode.

2.10 Angular Momentum

In the analytical model only particles on the x-axis with angular momentum $L = 0$ have been considered (results see figure 2.11, 2.12). The influence on halo production is highest for these $L = 0$ test-particles [1]. This will now be examined by solving (2.17) for all three directions directly without averaging or approximations made for test-particle motion, but with the same small mismatch approximation of the core motion (3 modes). The normalized angular momentum (analogous to [1]) is defined as

$$L = \frac{1}{a^2 q} \left| xy' - yx' \right| \tag{2.37}$$

where q is the depressed wave-number of the particles in the core, which can be calculated with Eq. (2.19) For simplicity the effect of angular momentum will be examined in a coasting beam in the transverse plane with equal radial and vertical tune. The particular choice of initial conditions corresponds to points on the positive x-axis in the right part of figure 2.3, thus we can examine the locations of the separatrices and the stable fix-point. An example for a trajectory of the latter case with $L > 0$ can be seen in figure 2.13. On the left side just a few turns are plotted and on the right side all turns are plotted to show the changes in the oscillation amplitude over a larger time-scale.

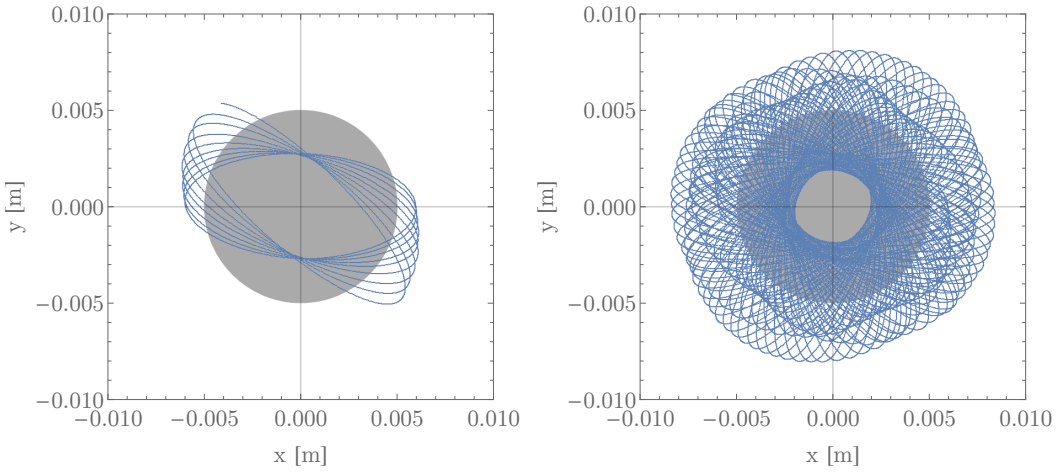

Figure 2.13: Trajectory of a single test-particle with angular momentum L = 0.95 in transverse plane for few turns (left) and 100 turns (right). The core is shown in gray.

For 100 turns, it is examined how the amplitude of the distance of the test-particle to the origin $r(t) = \sqrt{x^2(t) + y^2(t)}$ changes over time. The maximum $\max_t |r(t) - r(0)| =: \Delta r$ will be called Δr. Figure 2.14 depicts the dependence of

Δr on the initial amplitude $r(0)$ for different values of L. The changes in the test-particle amplitude are largest for $L = 0$ and decrease with growing L. Also, the location of the separatrix decreases. For a large enough L, the particle spends no time inside of the core and the effect of the resonance disappears (spherical bunch) or is very low (ellipsoidal bunch).

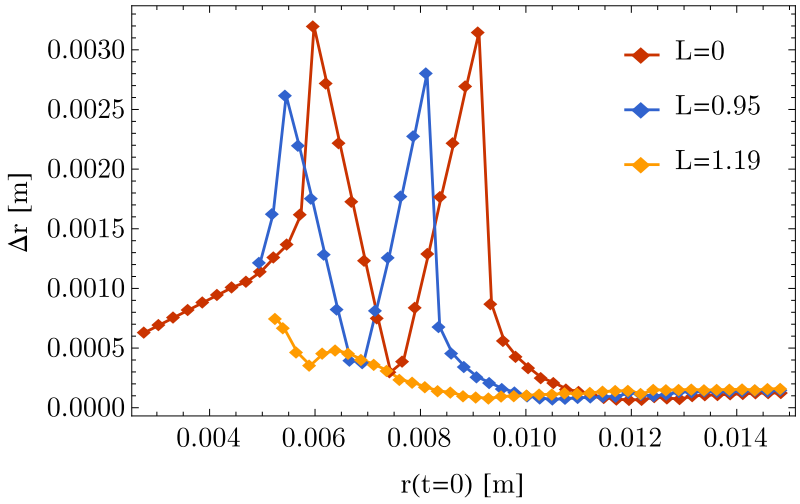

Figure 2.14: Effect of the angular momentum on the oscillations of the test-particle amplitudes, $r(t = 0)$ is the initial amplitude of the test-particle. The core radius was chosen to be 5 mm.

3 Full numerical particle-core model

The analytical model presented in chapter 2 introduced a few restrictions, eg. the test-particle motion was constrained to x-axis to allow for calculation of the times when the particles leave/enter the core, which is needed for averaging. Furthermore, the mismatch coefficients had to be given explicitly as input parameters. These can be difficult to estimate without running further simulations and therefore it would be an advantage have a model which consistently calculates the oscillations of the core. In a second particle-core model this will be achieved by also tracking some macro-particles of the core distributions in the focusing and space-charge field. The second moments of the distribution of the core macro-particles can then be used to calculate the semi-axes of the ellipsoidal core, which are used together with the total bunch charge or current to calculate the space-charge field of the core.

Given the fields, the motion of test and core particles is calculated from Eq. (2.17) with a Runge-Kutta method or 4th order. Dispersion is also included into the model by adding an additional dispersion term for the radial equation of motion. The focusing forces (without space charge) in all 3 directions are approximated as effective linear focusing forces, resulting in wave-numbers (=focusing constants) k_x, k_y and k_z respectively. In x and y direction (radial and vertical), these can be computed with the tunes and the revolution frequency. In longitudinal direction (z), k_z is chosen such that the space charge forces are compensated by the focusing and the bunch does not spread out in longitudinal direction.

3.1 Programming language, algorithms and libraries

C++: For speed reason, the model is implemented in C++(11), including *OpenMP* for efficient use of multiple cores.

Boost: The free *Boost C++ Libraries* are used for efficient ODE solving and reliable computation of special functions like elliptic integrals etc.

RK4: The fast and well-known Runge-Kutta algorithm of 4th order (RK4) is used to solve ODEs. It is implemented in the *Boost* libraries.

GSL: The GNU scientific library (*gsl*) is used to provide the values of physical constants.

3.2 Implementation Details

3.2.1 Calculation of core semi-axes from moments

For the calculation of the space-charge field, the core semi-axes a_x, a_y, a_z and the rotation angle ϕ in x, z plane are needed. They can be calculated from the second moments $\langle x^2\rangle, \langle y^2\rangle, \langle z^2\rangle$ and $\langle xz\rangle$, which can be computed from the distribution of representative core particles. As the bunch can be rotated by an angle ϕ, it is first brought to a new coordinate system, in which its semi-axes coincide with the axes of the coordinate system. In this rotated system, the field can be computed and then rotated back to the original coordinate system. The expressions for the semi-axes and the angle can be obtained by setting the second moment in the rotated system to zero. The formulas are explicitly given in [12]:

$$\begin{aligned}
\tan 2\phi &= \frac{2\langle xz\rangle}{\langle z^2\rangle - \langle x^2\rangle} \\
(a_x/k)^2 &= \frac{1}{2}\left[\langle x^2\rangle\left(1+\frac{1}{\cos 2\phi}\right) + \langle z^2\rangle\left(1-\frac{1}{\cos 2\phi}\right)\right] \\
(a_y/k)^2 &= \langle y^2\rangle \\
(a_z/k)^2 &= \frac{1}{2}\left[\langle x^2\rangle\left(1-\frac{1}{\cos 2\phi}\right) + \langle z^2\rangle\left(1+\frac{1}{\cos 2\phi}\right)\right]
\end{aligned} \tag{3.1}$$

where k is a distribution dependent factor and defined as

$$k = \left[\frac{1}{3}\int_0^\infty r^4 h(r^2)\mathrm{d}r\right]^{-1/2}, \tag{3.2}$$

for a distribution $h(r)$ that is normalized by

$$\int_0^\infty h(r^2)r^2\mathrm{d}r = 1\,. \tag{3.3}$$

It follows that for a KV distribution the factor equals to $k_{\mathrm{KV}} = \sqrt{5} \approx 2.236$

3.2.2 Test-particle motion

Every particle in a distribution is represented by the coordinates in it's 6 dimensional phase-space (x, p_x, y, p_y, z, p_z) in a local coordinate system, where the z direction points along the reference trajectory, x is radial and y is vertical direction. Positions are given in *meter* and momenta are given as corresponding unit-less $\beta\gamma$ for that direction.

The motion of the particle in a constant focusing channel with space charge (and no dispersion yet) can be described by the second order system of ODEs

$$\begin{aligned} x''(t) + k_x^2 x(t) &= \frac{q_e}{m_p} \cdot \vec{E}_{\mathrm{sc,x}}(x(t), y(t), z(t), t) \\ y''(t) + k_y^2 y(t) &= \frac{q_e}{m_p} \cdot \vec{E}_{\mathrm{sc,y}}(x(t), y(t), z(t), t) \\ z''(t) + k_z^2 z(t) &= \frac{q_e}{m_p} \cdot \vec{E}_{\mathrm{sc,z}}(x(t), y(t), z(t), t) \end{aligned} \tag{3.4}$$

has to be transformed into a system of first order ODEs for the boost ODE solver. for this purpose the new vector $\vec{r}$ is defined as

$$\vec{r} = \begin{pmatrix} r_1 \\ r_2 \\ r_3 \\ r_4 \\ r_5 \\ r_6 \end{pmatrix} = \begin{pmatrix} x\ [\mathrm{m}] \\ p_x[\beta\gamma] \\ y\ [\mathrm{m}] \\ p_y[\beta\gamma] \\ z\ [\mathrm{m}] \\ p_z[\beta\gamma] \end{pmatrix} \tag{3.5}$$

The momenta in the local frame (see figure 2.2) are small, so non-relativistic formula can be used. With elementary charge q_e and proton mass m_p they can be expressed as

$$p_x\,[\beta\gamma] = p_x\,[\mathrm{kg \cdot m/s}] \cdot \frac{1}{m_p[\mathrm{kg}] \cdot c[\mathrm{m/s}]} = \frac{x'[\mathrm{m/s}]}{c[\mathrm{m/s}]} \tag{3.6}$$

as unit-less relativistic parameters. Rearranging Eq. (3.6) and taking its derivative and plugging in Eq. (3.7) a first order inhomogeneous ODE for $\vec{r}$ can be derived which can be written in matrix form as

$$\vec{r}' = \begin{pmatrix} 0 & c & 0 & 0 & 0 & 0 \\ -k_x^2/c & 0 & 0 & 0 & 0 & 0 \\ 0 & 0 & 0 & c & 0 & 0 \\ 0 & 0 & -k_y^2/c & 0 & 0 & 0 \\ 0 & 0 & 0 & 0 & 0 & c \\ 0 & 0 & 0 & 0 & -k_z^2/c & 0 \end{pmatrix} \vec{r} + \frac{q_e}{m_p c} \begin{pmatrix} 0 \\ E_{\mathrm{sc,x}} \\ 0 \\ E_{\mathrm{sc,y}} \\ 0 \\ E_{\mathrm{sc,z}} \end{pmatrix} . \tag{3.7}$$

To add dispersion to the model, the radial equation has to be modified. ([4])

$$\frac{d^2}{ds^2} x = (\text{focusing}) + (\text{space charge}) + \frac{1}{\rho} \frac{p_z}{p_0} , \tag{3.8}$$

where p_0 is the reference momentum, ρ is the radius of the particle orbit and s the reference length on the orbit. The relation $\frac{d^2}{ds^2} = \frac{1}{\beta^2 c^2} \frac{d^2}{dt^2}$ is then used to rewrite the dispersion term with the time t as independent variable. For unit conversion purpose (momenta as $\beta\gamma$), the term has to be divided by another factor of c to yield in radial direction

$$r_2' = -\frac{k_x^2}{c} \cdot r_1 + \frac{q_e}{m_p c} E_x + \beta^2 c \frac{1}{p_0 \rho} \cdot r_6 \,. \tag{3.9}$$

Dispersion will introduce a coupling between the longitudinal momenta and the radial position.

One possibility to pass this equation to the boost ODE solver is to express it as a lambda expression in C++11 as shown in listing 3.1. All parameters of the core are implicitly passed via the capturing of a reference to the `EllipsoidalBunch core` object.

```
// 1 / (p * rho) * (unit conversion factor d2/ds2 ---> d2/dt2)
dispersion_term = (GSL_CONST_MKSA_SPEED_OF_LIGHT * beta) * (
    GSL_CONST_MKSA_SPEED_OF_LIGHT * beta) * (1.0 / reference_momentum)
    / radius;

auto ode = [&](std::vector<T>& x, std::vector<T>& dxdt, const T t) {
    std::vector<T> E(3);

    E = core.ElectricField(x[0], x[2], x[4], t);

    dxdt[0] = c * x[1];
    dxdt[1] = inv_c * (-kXSquared * x[0] + q_m * E[0]
              + dispersion_term * x[5]);
    dxdt[2] = c * x[3];
    dxdt[3] = inv_c * (-kYSquared * x[2] + q_m * E[1]);
    dxdt[4] = c * x[5];
    dxdt[5] = inv_c * (-kZSquared * x[4] + q_m * E[2]);
  };
};
```

Listing 3.1: Implementation of ODE as lambda expression

For each time-step in the integration the tracking of a core and a halo distribution is done in 3 steps:

- calculation of second moments of core distribution and semi-axes of KV core
- integration step core distribution
- integration step halo distribution

Halo particles are treated as test-particles in a sense they don't influence each other, opposed to the core macro-particles which influence each other and also the halo particles. The integration steps have to be done for many thousands of particles in the distribution and can be parallelized with OpenMP. For a quad-core system this lead to a speed-up factor of roughly 3.5. Apart from this, no further speed optimization has been done. The C++ code for this algorithm is given in listing 3.2.

```
//boost::numeric::odeint::runge_kutta4 stepper has no internal state
boost::numeric::odeint::runge_kutta4<std::vector<T> > stepper;

for (int i = 1; i < numSteps; i++) {
  T t1 = t;
  T dt1 = dt;

  //calculate new core dimensions from moments
  coreMoments =
    ParticleDistribution<T>::getSecondMoments(coreParticles);
  T core_phi =
    EllipsoidalBunch<T>::calculatePhiFromMoments(coreMoments);

  core_ax = sqrt(0.5 * (coreMoments[0] * (1.0 + 1.0 / cos(2.0 *
    core_phi)) + coreMoments[4] * (1.0 - 1.0 / cos(2.0 * core_phi)))) *
    KV_RADIUS_MOMENT_FACTOR;
  core_ay = sqrt(coreMoments[2]) * KV_RADIUS_MOMENT_FACTOR;
  core_az = sqrt(0.5 * (coreMoments[0] * (1.0 - 1.0 / cos(2.0 *
    core_phi)) + coreMoments[4] * (1.0 + 1.0 / cos(2.0 * core_phi)))) *
    KV_RADIUS_MOMENT_FACTOR;

  core.setDimensions(core_ax, core_ay, core_az, core_phi);

  //track core
#pragma omp parallel for default(none) shared(coreParticles)
    firstprivate(t1, dt1, ode, stepper)
  for (int i = 0; i < coreDistribution.numParticles; i++) {
    stepper.do_step(ode, coreParticles[i].phaseSpaceCoords, t1, dt1);
  }

  //track halo particles
#pragma omp parallel for default(none) shared(haloParticles)
    firstprivate(t1, dt1, ode, stepper)
  for (int i = 0; i < haloDistribution.numParticles; i++) {
    stepper.do_step(ode, haloParticles[i].phaseSpaceCoords, t1, dt1);
  }

  t += dt;
}
```

Listing 3.2: Combined tracking of core and halo

To calculate the E-field of the core, the `ode` lambda expression relies on the `EllipsoidalBunch<T>::ElectricField` member function which directly uses the simple analytical expression (Eq. 2.8) to calculate the field inside the core or uses the negative numerical derivative of `EllipsoidalBunch<T>::ElectrostaticPotential` for particles outside the core, because the analytical expression would be require more evaluations.

```cpp
template <class T >
std::vector<T> EllipsoidalBunch<T>::ElectricField(T x, T y, T z, T t){
  std::vector<T> E0(3), E(3);
  T as = _ax*_ax, bs = _ay*_ay, cs = _az*_az;
  T xs = x*x, ys = y*y, zs = z*z;

  if ((xs / as + ys / bs + zs / cs <= 1.0)) {
    T gamma = 1.0 / sqrt(1.0 - (_beta*_beta));

    //preFactor: Q / (4 pi e0)
    T preFactor = _bunchCharge / (4.0 * M_PI *
    GSL_CONST_MKSA_VACUUM_PERMITTIVITY);

    E0[0] = preFactor * (x * boost::math::ellint_rd(bs, cs, as));
    E0[1] = preFactor * (y * boost::math::ellint_rd(cs, as, bs));
    E0[2] = preFactor * (z * boost::math::ellint_rd(as, bs, cs));
  } else {
    //derivative has to be calculated with SYMMETRIC secant!!!
    T h = 5e-7;
    E0[0] = -(ElectrostaticPotential(x + h, y, z, t) -
    ElectrostaticPotential(x - h, y, z, t)) / (2 * h);
    E0[1] = -(ElectrostaticPotential(x, y + h, z, t) -
    ElectrostaticPotential(x, y - h, z, t)) / (2 * h);
    E0[2] = -(ElectrostaticPotential(x, y, z + h, t) -
    ElectrostaticPotential(x, y, z - h, t)) / (2 * h);
  }

  //in real (x,z) coordinate system \ => phi negative, / => phi
    positive. In rotated system: always |
  T cos_phi = cos(_phi);
  T sin_phi = sin(_phi);

  //rotate back
  E[0] = cos_phi * E0[0] + sin_phi * E0[2];
  E[1] = E0[1];
  E[2] = -sin_phi * E0[0] + cos_phi * E0[2];

  return E;
}
```

Listing 3.3: Calculation of electric field of ellipsoidal bunch

```cpp
template <class T >
T EllipsoidalBunch<T>::ElectrostaticPotential(T x, T y, T z, T t){
  T as = _ax*_ax, bs = _ay*_ay, cs = _az*_az;
  T xs = x*x, ys = y*y, zs = z*z;

  T gamma = 1.0 / sqrt(1.0 - (_beta*_beta));

  //preFactor: Q / (4 pi epsilon0)
  T preFactor = _bunchCharge / (4.0 * M_PI *
   GSL_CONST_MKSA_VACUUM_PERMITTIVITY);

  if (xs / as + ys / bs + zs / cs <= 1.0) {
    //calculate potential
    return  preFactor * 3.0 / 2.0 * (
      boost::math::ellint_rf(cs, bs, as)
      - xs / 3.0 * boost::math::ellint_rd(bs, cs, as)
      - ys / 3.0 * boost::math::ellint_rd(cs, as, bs)
      - zs / 3.0 * boost::math::ellint_rd(as, bs, cs)
    );

  } else {
    // x^2/(a^2+s) + y^2/(b^2+s) + z^2/(c^2+s) - 1 == 0    (*)
    // -> s^3 + A s^2 + B s + C == 0                (**)
    T A = as + bs + cs - xs - ys - zs;
    T B = -(cs*(xs + ys)) + bs*(cs - xs - zs) + as*(bs + cs - ys - zs);
    T C = -(bs*cs*xs) - as*(cs*ys + bs*(-cs + zs));

    //solve equation (**)
    T lambda = NumericalMethods<T>::cubicLargestRoot(A, B, C);

    //calculate potential
    return preFactor * 3.0 / 2.0 * (
      boost::math::ellint_rf(as + lambda, bs + lambda, cs + lambda)
      - (xs * boost::math::ellint_rd(bs + lambda, cs + lambda, as +
   lambda)) / 3.0
      - (ys * boost::math::ellint_rd(cs + lambda, as + lambda, bs +
   lambda)) / 3.0
      - (zs * boost::math::ellint_rd(as + lambda, bs + lambda, cs +
   lambda)) / 3.0
    );
  }
}
```

Listing 3.4: Calculation of electrostatic potential of ellipsoidal bunch

3.3 Results

3.3.1 Core

With the numerical particle-core model the evolution of the core can be tracked. As a first example a coasting beam without dispersion is analyzed. The other parameters of the machine (current, tunes etc.) are taken similar to Injector 2 (see TEST07 table in appendix). The result can be seen in figure 3.7, all three semi-axes of the core oscillate around an approximately constant mean value. By looking at the spectrum of these oscillations (figure 3.2), three dominant peaks can be identified, which are at the same location in all 3 directions but with quite different peak heights.

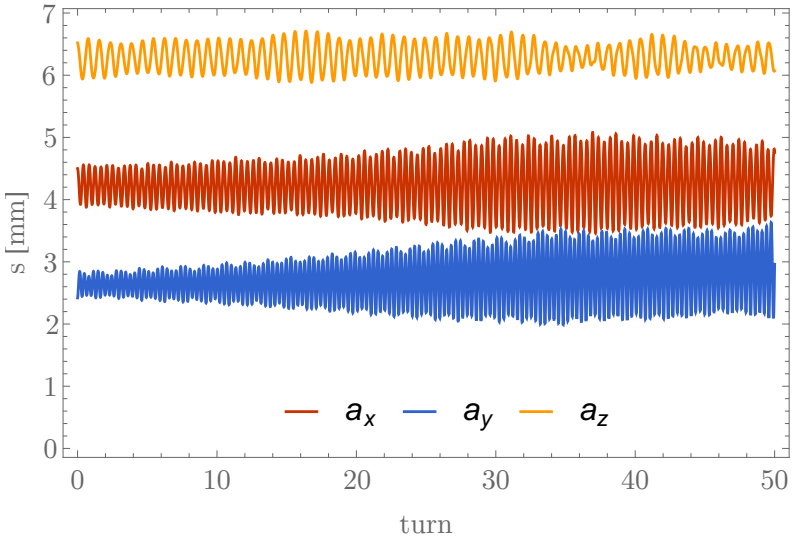

Figure 3.1: Core semi-axes as function of time, calculated with particle-core model without dispersion for coasting beam at 30 MeV

To study the effects of dispersion and acceleration the simulations is done again for the TEST08 example, including dispersion. It can be seen in figure 3.3, that the mean value of the oscillations changes over time, too.

3.3.2 Test-particle distributions

The numerical particle-core model can now be applied to several test-cases. At first the TEST08 parameters used, which are mostly like the ones of Injector 2, including dispersion. For the coasting beam case, an unmatched distribution is studied at 30 MeV which leads to a halo with a large extend in x and z. The phase-space (left) and real space (right) can be seen in figure 3.4. Figure 3.5 depicts the same simulation for an accelerated beam, where a distribution with the same moments than a matched distribution of injector 2 was used. Since not all properties of the test machine and the Injector 2 are the same, there might be better matched

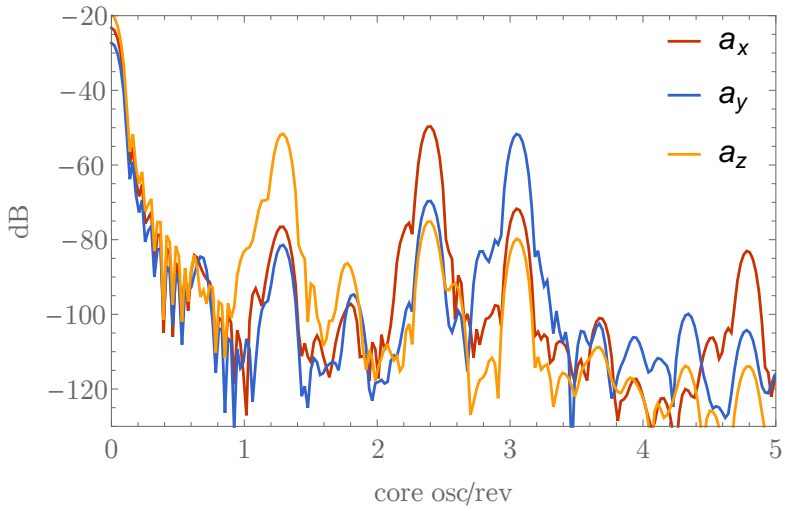

Figure 3.2: Power spectrum of core semi-axes oscillation of figure 3.7. Oscillation in all three directions contains the same three frequencies, but with different peak heights.

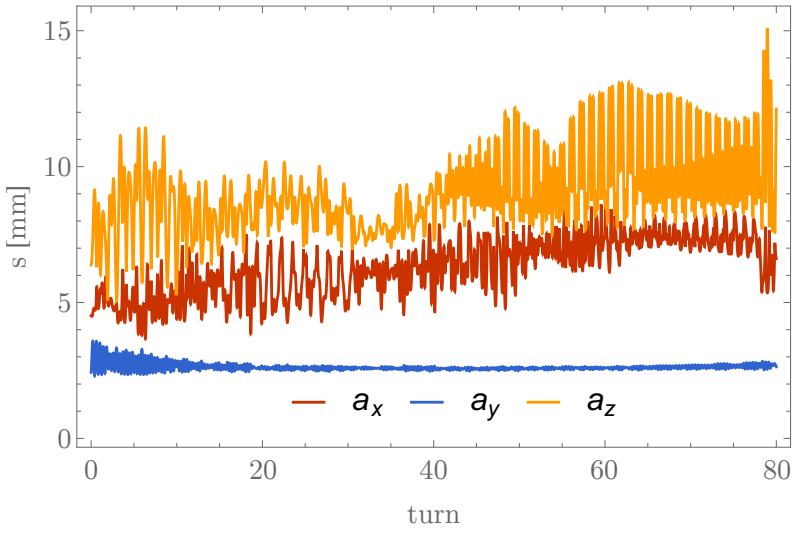

Figure 3.3: Core semi-axes as function of time, calculated with particle-core model for Injector 2 like machine TEST08 with dispersion and acceleration.

distributions for the test-machine. After 80 turns, a beam halo, mostly in radial direction can be observed, too. In vertical direction, no halo was observed. The simulations used 10000 representative core particles to have enough statistics to calculate the core moments.

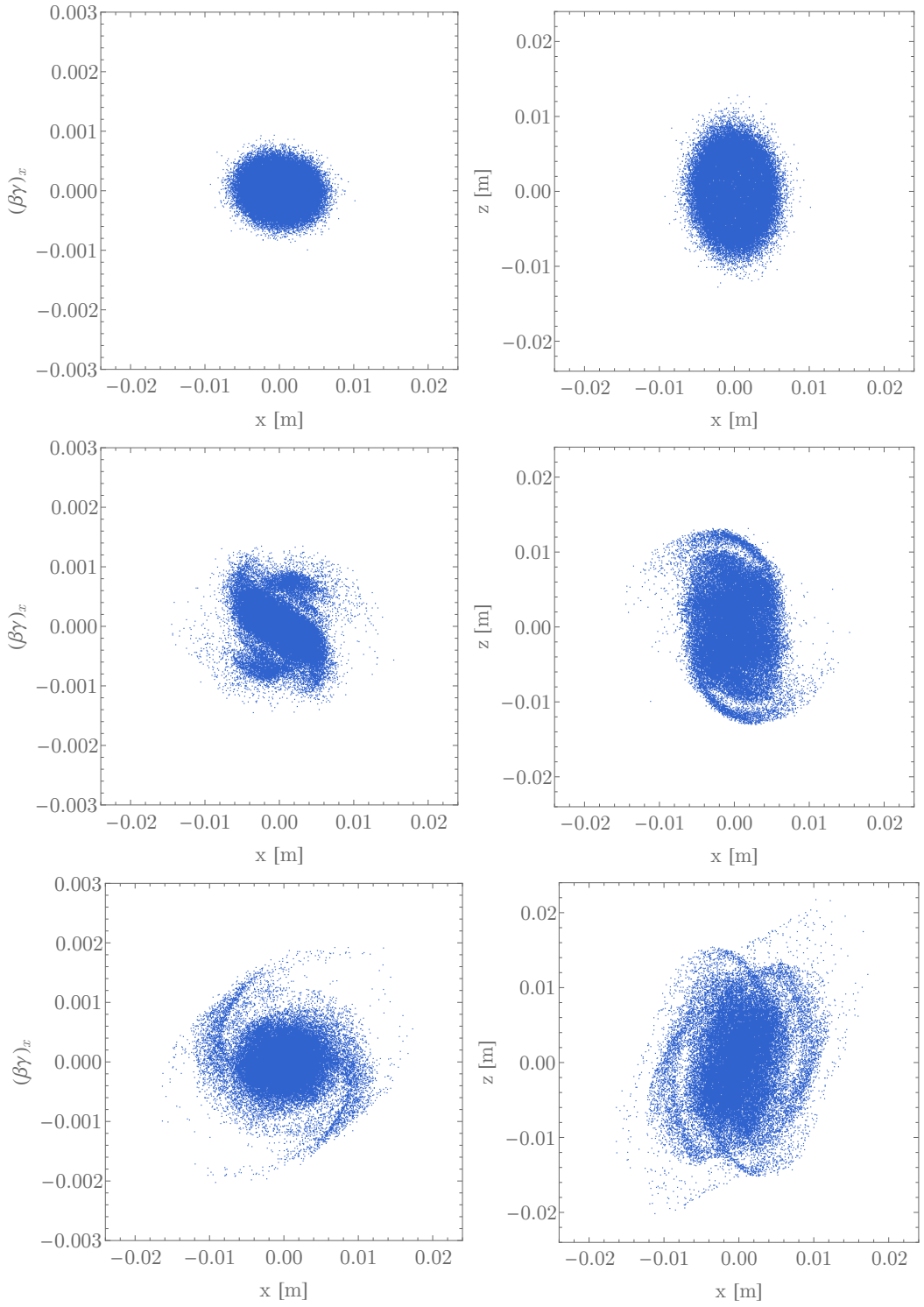

Figure 3.4: Phase-space x, p_x (left) and real space x, z (right), at starting point (top), after 10 turns (middle) an after 40 turns (bottom). Injector 2 like machine TEST2 with dispersion, **coasting beam at 30 MeV** with 2.5 mA current, 5000 test-particles

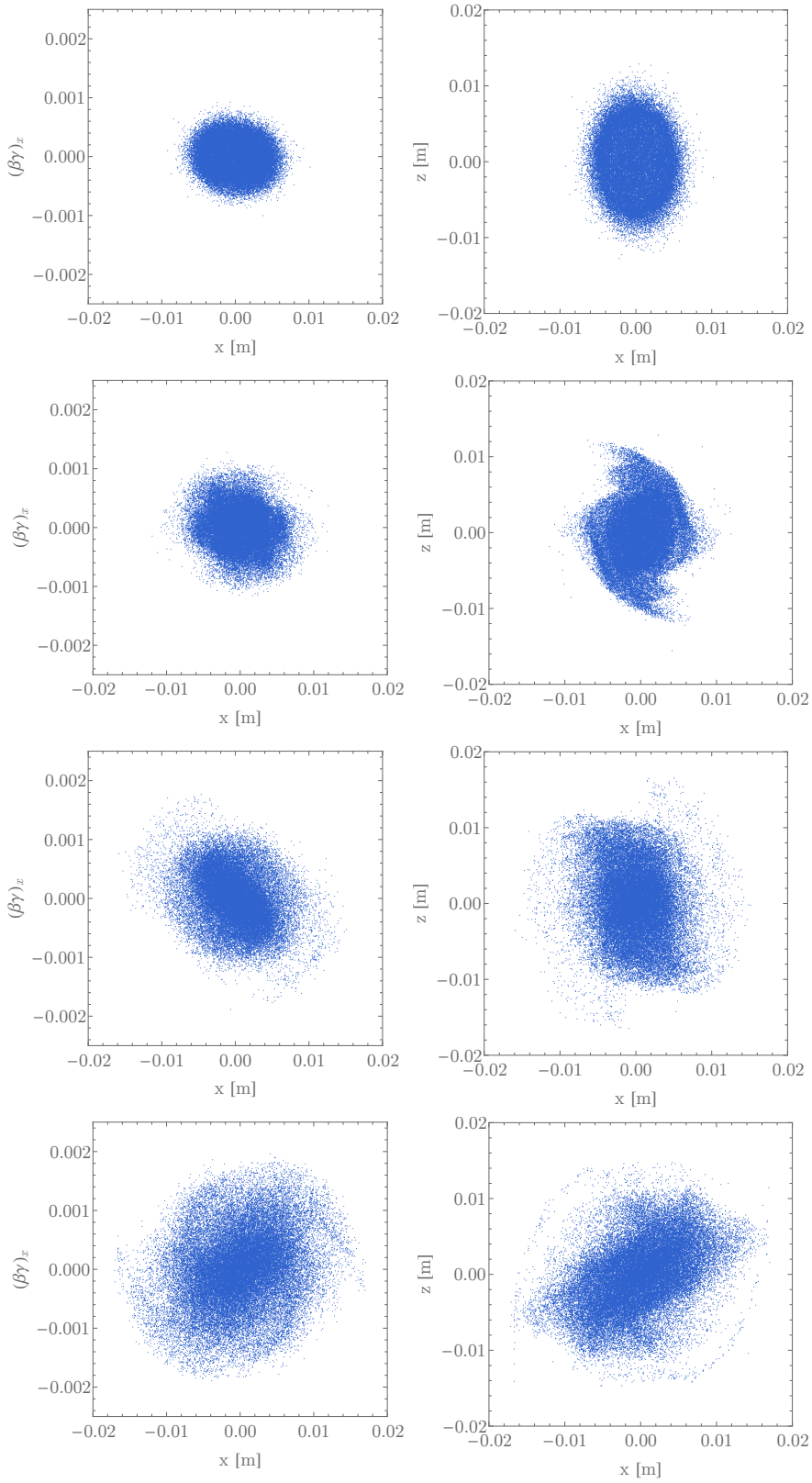

Figure 3.5: Phase-space x, p_x (left) and real space x, z (right), at initial time (top), after 10 turns, after 40 turns and after 80 turns (bottom). Injector 2 like machine TEST08 with dispersion, 2.4mA current, 40000 test-particles

In the tails of the core, the density of particles is increased over time as can be seen in figure 3.5. Compared to 2.12, there is no "ring" visible in phase-space. This could be attributed to the different angular momenta of the particles, as it has been shown that the position of the critical points for stability depends on the angular momenta. Another reason could be the dispersion. Instead, there is a whole region of test-particles formed around the core in phase-space as well as in real space. The histogram of x positions is shown in figure 3.6.

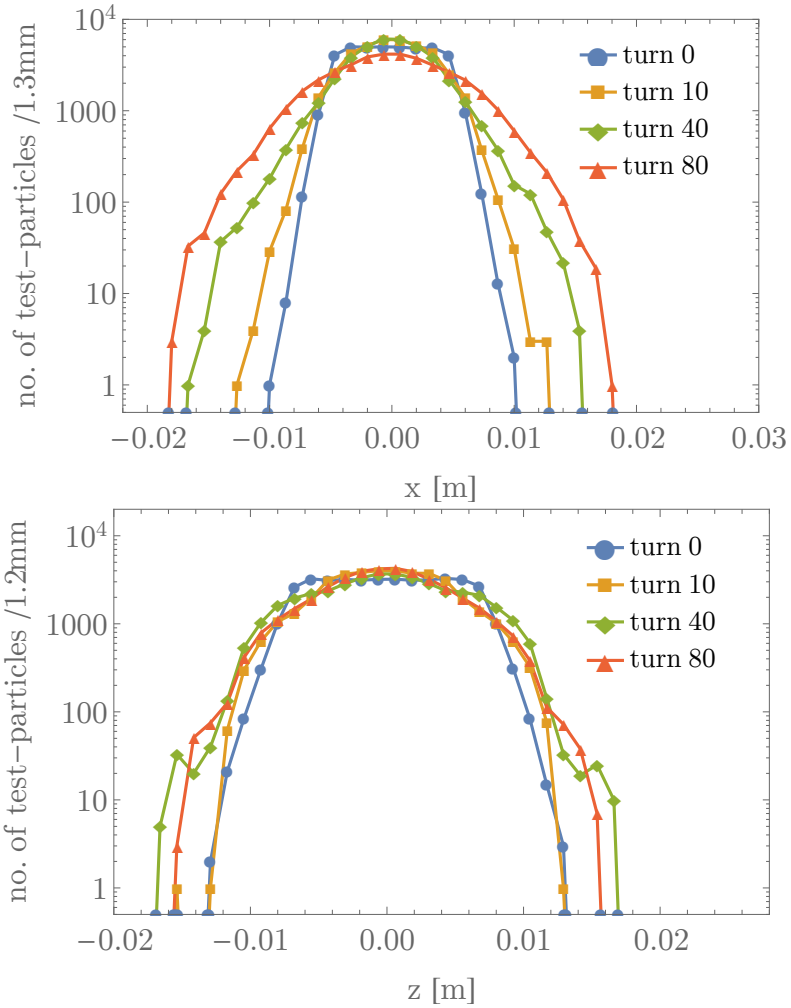

Figure 3.6: Histogram of radial (top) and longitudinal (bottom) positions after different turns. Only test-particles are considered, no core particles. In vertical direction almost no change is observed.

Limits for the validity of this model can be found by examining the distribution of the representative core particles. If after a certain time, it is too different from the assumed distribution (eg. KV), then the field calculated from the moments will differ from the reals field.

3.3.3 Comparison with analytical model

Both models derived in this thesis can now be applied to a simple case for comparison. The simple machine TEST1 (see table B.1) with a coasting beam is used. The initial distribution is chosen in a way such that the numeric model predicts small (order of 10 %) oscillations in all core semi-axes. The mean values and amplitudes of the core semi-axes oscillations are then used as input parameters for the analytic model and are assumed constant for simplicity, although in the outcome (figure 3.7) of the numeric model they were slightly changing. All test-particles have been initialized with zero angular momentum for the analytic model to be applicable.

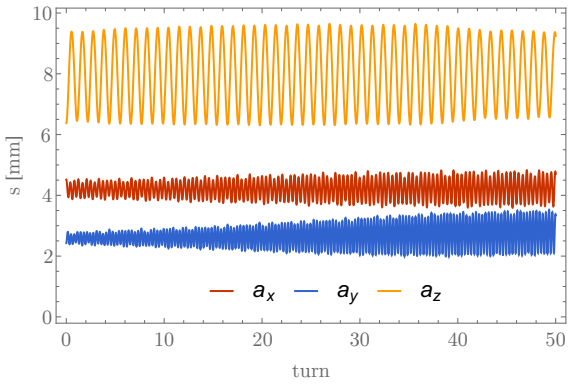

Figure 3.7: Core oscillations for a coasting beam at 30 MeV without dispersion.

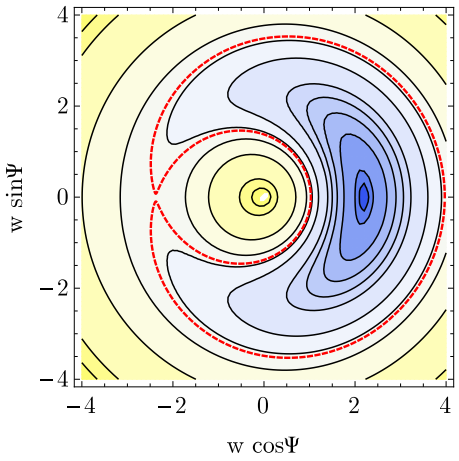

Figure 3.8: w, Ψ phase-space for a coasting beam at 30 MeV without dispersion, separatrix is red and dashed. Critical/fixed points are A = 2.38, B = 1.03, C = 2.19, D = 3.96.

Then the analytical model with the so obtained mismatch coefficients is used to produce a phase-space plot in w, Ψ showing the separatrix. Furthermore to illustrate

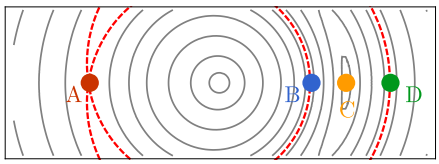

points:
A: unstable fix-point
B: inner separatrix
C: stable fix-point
D: outer separatrix

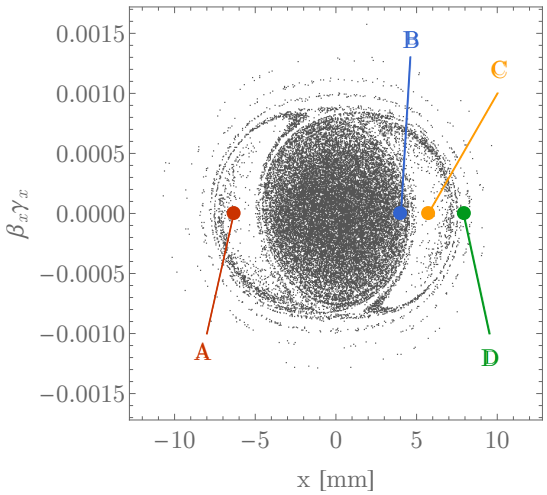

Figure 3.9: Naming convention of phase-space in analytic model (left), x, p_x phase-space after 40 turns, calculated with numeric model shown with characteristic phase-space points calculated with analytic model. (right)

x, p_x phase space the analytic model is also used to track a distribution of particles. Both calculations can be seen in figure 3.10. The results look quite similar in x, but have different extend in p_x direction. Furthermore the phase-space is a bit rotated, which could be attributed to the error in time-scale that comes from averaging. The differences can be attributed to the various approximations made in the analytical model (eg. small, constant mismatch and Taylor expansion of elliptic integrals) and still too different initial conditions.

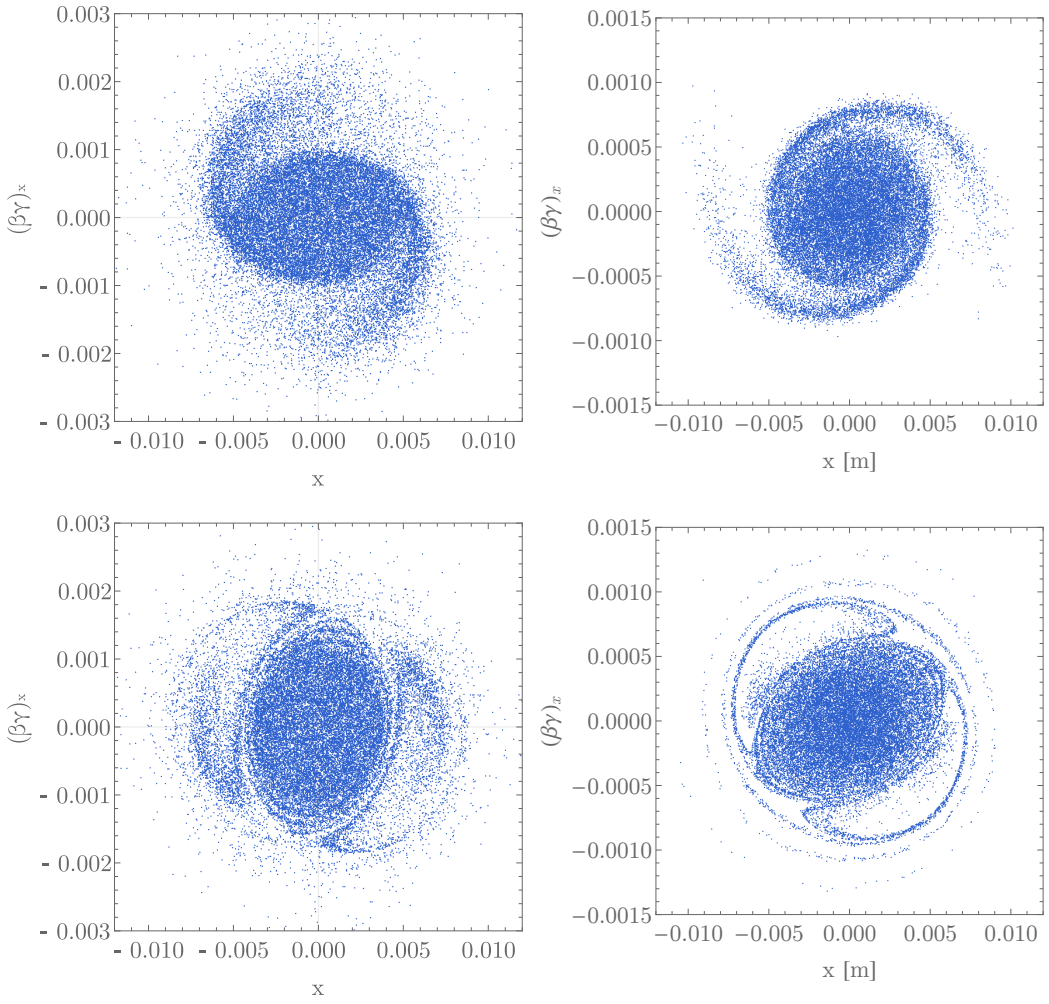

Figure 3.10: Comparison of analytical model (left) and new numerical model (right) for a test-particle distribution with $L = 0$ after 5 turns (top) and 27 turns (bottom).

4 Summary and Conclusion

The analytical particle-core model of Gluckstern has been extended to bunched beams with ellipsoidal bunches including the small-mismatch core motion consisting of three independent modes (quadrupole, high and low mode) derived by Bongard and Pabst. Acceleration also has been taken into account. This model can be used for a better understanding of the theory of halo formation by parametric resonance. Assuming realistic machine parameters, as in the original model [1] a separation of phase space in three regions has been observed. In one of these regions (eg. shown in orange on the right side of figure 2.4), the amplitude of test particle oscillations undergoes large changes over time which can be seen as one cause for halo formation. In the analytical model derived in chapter 2 some simplifications had to be made in order to allow for an analytic calculation of the constants of motion, e.g the test-particles have zero angular momentum (and therefore the halo formation is over-estimated) and the oscillation of the core semi-axis have to be small, which might not be the case for a badly matched distribution. Furthermore the elliptic integrals have been approximated by Taylor series. The coefficients of the mismatch modes have to be given in advance as input parameters. The model was then be used for a *coasting* and an *accelerated* beam and the influence of acceleration was studied. The acceleration caused a change in parameters (γ an also indirectly the tunes as the orbit changes) which changed the location of the separatrix and the three regions in phase-space (see section 2.6). This lead to particles changing the region and new effects compared to the coasting beam case.

To overcome the limitations of the analytical model, a new particle-core model has been developed. Instead of specifying the core motion as input parameter, it will be calculated by tracking a distribution of macro particles. Therefore it requires two distributions (one for the core and one for the halo) as input and then tracks both core and test-particles with the same equations in the field of the core. This field is calculated from a uniform KV core, of which the parameters (semi-axes, rotation angle) were computed from the second moments of the core distribution. This ensured, that core and test-particles were treated consistently without having to refer to other simulations/results. The focusing in this model is approximated by a field linear in each direction and dispersion is also added to the model. The new model was then applied to a machine with similar parameters (e.g. tunes, energies) as PSI injector 2, but with a simple classical cyclotron shape. It has been observed that the core performs oscillations in all three directions and also can rotate around the vertical axis. A significant formation and growth of halo was observed too, depending on the beam current. In phase-space as well as in real space, a spiral structure is seen in the distribution, which is a sign of the non-linearities in

the model which are the result of the non-linear space-charge forces on the outside of the core. The effect of angular momentum could also be examined using the numeric model, because in the analytic model the calculation of the times when the test-particle leaves/enters the core is not possible in the general case of non equal tunes in the different directions.

A possible extension of the model would be using real measured field maps for magnets and cavities instead of using the tune map for the focusing and increasing the energy in a single step per turn. In this way, phase-focusing for the longitudinal direction could be consistently implemented and the effects of the geometry could be examined instead of approximating the orbits as round. Quantitative analysis of beam halo could be done using a real number of particles in the tails of the distribution and relating the number of core macro particles to the real number of core particles. The model could be implemented in an existing particle-tracking code like OPAL for convenient use. In terms of speed, the calculation of the elliptic integrals, which now takes most of the CPU time, could be replaced by faster algorithms if they exist or fast approximations with lower precision, if this has no influence on the result. The model could also be extended towards more realistic particle distributions for the core, eg. Gaussian, parabolic or any other parametric distributions.

5 Acknowledgement

I would like to thank the ETH, the PSI, all colleagues from the AMAS group and especially my supervisor Dr. Andreas Adelmann for their kind support during my thesis.

Part I

Appendix

A Formulas

In the derivation above formulas were only given up to order 2 in the bunch eccentricities e, f. To make the terms shorter, $g = \sqrt{w-1}$ has been defined. The formulas up to order 8 are:

$$\widetilde{W}_{\mathrm{h}}(w) = \begin{cases} \frac{\tilde{C}_{\mathrm{ih}} w}{2a_z^2} & \text{if } w \leq 1 \\ \frac{1}{\pi a_z^2}\Big(- \frac{\tilde{C}_{\mathrm{o10h}}\big(g\big(-48w^3+8w^2+10w+15\big)+15\log\big(g+\sqrt{w}\big)/\sqrt{w}\big)}{48(1-e^2)^{11/2}w^4} & \text{if } w > 1 \\ - \frac{\tilde{C}_{\mathrm{o12h}}\big(g\big(-384w^4+48w^3+56w^2+70w+105\big)+105\log\big(g+\sqrt{w}\big)/\sqrt{w}\big)}{480(1-e^2)^{13/2}w^5} \\ + \frac{2\tilde{C}_{\mathrm{o4h}}\big(2g\sqrt{w}+w\log\big(\sqrt{w}-g\big)+(w-2)\log\big(g+\sqrt{w}\big)\big)}{(1-e^2)^{5/2}w^{3/2}} + \frac{\tilde{C}_{\mathrm{o6h}}\Big(2g\sqrt{w^3}-g\sqrt{w}+\log\Big(\frac{-g+\sqrt{w}+1}{g+\sqrt{w}+1}\Big)\Big)}{(1-e^2)^{7/2}w^{5/2}} \\ - \frac{\tilde{C}_{\mathrm{o8h}}\big(g\big(-8\sqrt{w^5}+2\sqrt{w^3}+3\sqrt{w}\big)-3\log\big(\sqrt{w}-g\big)\big)}{6(1-e^2)^{9/2}w^{7/2}} + \frac{\tilde{C}_{\mathrm{ih}}\big(g\big(\frac{4}{w}-2\big)-2w\tan^{-1}(g)+\pi w\big)}{2}\Big) \end{cases} \tag{A.1}$$

The other auxiliary functions $\widetilde{W}$ can be obtained by replacing 'h' with either 'q' or 'l' in the coefficients of the above expression (A.1). The $\tilde{P}$ auxiliary functions are the derivatives with respect to w of the $\widetilde{W}$ functions and $\widetilde{W}_0$ is defined as:

$$\widetilde{W}_0(w) = \tag{A.2}$$

$$\begin{cases} \frac{854992e^8-32e^6\big(7759f^2+91356\big)+192e^4\big(761f^4+1779f^2+21060\big)+8407f^8+12264f^6+19440f^4+60480f^2}{226800a_z^2(1-e^2)^{11/2}} & \text{if } w \leq 1 \\ - \frac{+8e^2\big(6979f^6+10278f^4+29160f^2+317520\big)-604800}{226800a_z^2(1-e^2)^{11/2}} \\ \frac{4\big(2e^2-f^2\big)\sqrt{w-e^2w}\Big(\sqrt{w}\Big(g+2w\sin^{-1}\Big(\frac{1}{\sqrt{w}}\Big)\Big)+\sinh^{-1}(g)\Big)}{15\pi a_z^2(e^2-1)^3w^2} & \text{if } w > 1 \\ + \frac{16\Big(\sinh^{-1}(g)+\sqrt{w}\sin^{-1}\Big(\frac{1}{\sqrt{w}}\Big)\Big)}{3\pi a_z^2(1-e^2)^{3/2}\sqrt{w}} \\ + \frac{\big(8e^4-8e^2f^2+3f^4\big)\Big(2g\sqrt{w^3}+3g\sqrt{w}+3\sinh^{-1}(g)+8w^{5/2}\sin^{-1}\Big(\frac{1}{\sqrt{w}}\Big)\Big)}{140\pi a_z^2(1-e^2)^{7/2}w^{5/2}} \\ + \frac{\big(1420e^4-1420e^2f^2+1201f^4\big)\big(f^2-2e^2\big)^2\Big(g\sqrt{w}\big(48w^3+56w^2+70w+105\big)+105\sinh^{-1}(g)+384w^{9/2}\sin^{-1}\Big(\frac{1}{\sqrt{w}}\Big)\Big)}{6220800\pi a_z^2(1-e^2)^{11/2}w^{9/2}} \\ - \frac{\big(224e^6-336e^4f^2+258e^2f^4-73f^6\big)\Big(g\big(8\sqrt{w^5}+10\sqrt{w^3}+15\sqrt{w}\big)+15\sinh^{-1}(g)+48w^{7/2}\sin^{-1}\Big(\frac{1}{\sqrt{w}}\Big)\Big)}{32400\pi a_z^2(1-e^2)^{9/2}w^{7/2}} \\ + \frac{\big(15309e^8+756e^6\big(9f^2+22\big)+18e^4\big(315f^4+364f^2+1000\big)\big)\big((w-2)\tan^{-1}(g)+g\big)}{16800\pi a_z^2} \\ + \frac{\big(36e^2\big(105f^6+154f^4+200f^2+560\big)+693f^8+1736f^6+3600f^4+6720f^2+22400\big)\big((w-2)\tan^{-1}(g)+g\big)}{16800\pi a_z^2} \end{cases} \tag{A.3}$$

The coefficients with tildes are listed in table A.1 and table A.2. For constant mismatch parameters and mean core dimensions over the time interval of interest, these coefficients only have to be calculated once.

$$
\begin{array}{l|l}
\tilde{C}_{\mathrm{o4h}} & -\frac{2C_{\mathrm{hl}}}{5}-\frac{4C_{\mathrm{hr}}e^2}{5}+\frac{4C_{\mathrm{hr}}}{5}+\frac{2C_{\mathrm{hv}}f^2}{5}-\frac{2C_{\mathrm{hv}}}{5}\\
\tilde{C}_{\mathrm{o4q}} & -\frac{4C_{\mathrm{qr}}e^2}{5}+\frac{4C_{\mathrm{qr}}}{5}-\frac{2C_{\mathrm{qv}}f^2}{5}+\frac{2C_{\mathrm{qv}}}{5}\\
\tilde{C}_{\mathrm{o4l}} & \frac{2C_{\mathrm{ll}}}{5}-\frac{4C_{\mathrm{lr}}e^2}{5}+\frac{4C_{\mathrm{lr}}}{5}+\frac{2C_{\mathrm{lv}}f^2}{5}-\frac{2C_{\mathrm{lv}}}{5}\\
\tilde{C}_{\mathrm{o6h}} & e^2\left(\frac{4C_{\mathrm{hl}}}{7}+f^2\left(-\frac{4C_{\mathrm{hr}}}{7}-\frac{4C_{\mathrm{hv}}}{7}\right)-\frac{8C_{\mathrm{hr}}}{7}+\frac{4C_{\mathrm{hv}}}{7}\right)+f^2\left(-\frac{C_{\mathrm{hl}}}{7}+\frac{4C_{\mathrm{hr}}}{7}-\frac{3C_{\mathrm{hv}}}{7}\right)+\frac{8C_{\mathrm{hr}}e^4}{7}+\frac{3C_{\mathrm{hv}}f^4}{7}\\
\tilde{C}_{\mathrm{o6q}} & e^2\left(f^2\left(\frac{4C_{\mathrm{qv}}}{7}-\frac{4C_{\mathrm{qr}}}{7}\right)-\frac{8C_{\mathrm{qr}}}{7}-\frac{4C_{\mathrm{qv}}}{7}\right)+f^2\left(\frac{4C_{\mathrm{qr}}}{7}+\frac{3C_{\mathrm{qv}}}{7}\right)+\frac{8C_{\mathrm{qr}}e^4}{7}-\frac{3C_{\mathrm{qv}}f^4}{7}\\
\tilde{C}_{\mathrm{o6l}} & e^2\left(-\frac{4C_{\mathrm{ll}}}{7}+f^2\left(-\frac{4C_{\mathrm{lr}}}{7}-\frac{4C_{\mathrm{lv}}}{7}\right)-\frac{8C_{\mathrm{lr}}}{7}+\frac{4C_{\mathrm{lv}}}{7}\right)+f^2\left(\frac{C_{\mathrm{ll}}}{7}+\frac{4C_{\mathrm{lr}}}{7}-\frac{3C_{\mathrm{lv}}}{7}\right)+\frac{8C_{\mathrm{lr}}e^4}{7}+\frac{3C_{\mathrm{lv}}f^4}{7}\\
\tilde{C}_{\mathrm{o8h}} & e^4\left(-\frac{196C_{\mathrm{hl}}}{225}+f^2\left(\frac{392C_{\mathrm{hr}}}{225}+\frac{196C_{\mathrm{hv}}}{225}\right)+\frac{392C_{\mathrm{hr}}}{225}-\frac{196C_{\mathrm{hv}}}{225}\right)+e^2\left(f^2\left(\frac{91C_{\mathrm{hl}}}{225}-\frac{392C_{\mathrm{hr}}}{225}+\frac{301C_{\mathrm{hv}}}{225}\right)\right.\\
& \left.+f^4\left(-\frac{301C_{\mathrm{hr}}}{450}-\frac{301C_{\mathrm{hv}}}{225}\right)\right)+f^4\left(-\frac{91C_{\mathrm{hl}}}{900}+\frac{301C_{\mathrm{hr}}}{450}-\frac{511C_{\mathrm{hv}}}{900}\right)-\frac{392C_{\mathrm{hr}}e^6}{225}+\frac{511C_{\mathrm{hv}}f^6}{900}\\
\tilde{C}_{\mathrm{o8q}} & e^4\left(f^2\left(\frac{392C_{\mathrm{qr}}}{225}-\frac{196C_{\mathrm{qv}}}{225}\right)+f^4\left(\frac{301C_{\mathrm{qr}}}{450}+\frac{511C_{\mathrm{qv}}}{900}\right)-\frac{392C_{\mathrm{qr}}e^6}{225}-\frac{511C_{\mathrm{qv}}f^6}{900}\right.\\
& \left.+\frac{392C_{\mathrm{qr}}}{225}+\frac{196C_{\mathrm{qv}}}{225}\right)+e^2\left(f^4\left(\frac{301C_{\mathrm{qv}}}{225}-\frac{301C_{\mathrm{qr}}}{450}\right)+f^2\left(-\frac{392C_{\mathrm{qr}}}{225}-\frac{301C_{\mathrm{qv}}}{225}\right)\right)\\
\tilde{C}_{\mathrm{o8l}} & e^4\left(\frac{196C_{\mathrm{ll}}}{225}+f^2\left(\frac{392C_{\mathrm{lr}}}{225}+\frac{196C_{\mathrm{lv}}}{225}\right)+\frac{392C_{\mathrm{lr}}}{225}-\frac{196C_{\mathrm{lv}}}{225}\right)+f^4\left(\frac{91C_{\mathrm{ll}}}{900}+\frac{301C_{\mathrm{lr}}}{450}-\frac{511C_{\mathrm{lv}}}{900}\right)\\
& +e^2\left(f^2\left(-\frac{91C_{\mathrm{ll}}}{225}-\frac{392C_{\mathrm{lr}}}{225}+\frac{301C_{\mathrm{lv}}}{225}\right)+f^4\left(-\frac{301C_{\mathrm{lr}}}{450}-\frac{301C_{\mathrm{lv}}}{225}\right)\right)-\frac{392C_{\mathrm{lr}}e^6}{225}+\frac{511C_{\mathrm{lv}}f^6}{900}\\
\tilde{C}_{\mathrm{o10h}} & e^6\left(\frac{71C_{\mathrm{hl}}}{45}+f^2\left(-\frac{71C_{\mathrm{hr}}}{15}-\frac{71C_{\mathrm{hv}}}{45}\right)-\frac{142C_{\mathrm{hr}}}{45}+\frac{71C_{\mathrm{hv}}}{45}\right)+f^6\left(-\frac{71C_{\mathrm{hl}}}{360}+\frac{389C_{\mathrm{hr}}}{450}-\frac{1201C_{\mathrm{hv}}}{1800}\right)\\
& +e^4\left(f^2\left(-\frac{107C_{\mathrm{hl}}}{75}+\frac{71C_{\mathrm{hr}}}{15}-\frac{248C_{\mathrm{hv}}}{75}\right)+f^4\left(\frac{248C_{\mathrm{hr}}}{75}+\frac{248C_{\mathrm{hv}}}{75}\right)\right)\\
& +e^2\left(f^4\left(\frac{107C_{\mathrm{hl}}}{150}-\frac{248C_{\mathrm{hr}}}{75}+\frac{389C_{\mathrm{hv}}}{150}\right)+f^6\left(-\frac{389C_{\mathrm{hr}}}{450}-\frac{389C_{\mathrm{hv}}}{150}\right)\right)+\frac{142C_{\mathrm{hr}}e^8}{45}+\frac{1201C_{\mathrm{hv}}f^8}{1800}\\
\tilde{C}_{\mathrm{o10q}} & e^6\left(f^2\left(\frac{71C_{\mathrm{qv}}}{45}-\frac{71C_{\mathrm{qr}}}{15}\right)-\frac{142C_{\mathrm{qr}}}{45}-\frac{71C_{\mathrm{qv}}}{45}\right)+e^4\left(f^4\left(\frac{248C_{\mathrm{qr}}}{75}-\frac{248C_{\mathrm{qv}}}{75}\right)+f^2\left(\frac{71C_{\mathrm{qr}}}{15}+\frac{248C_{\mathrm{qv}}}{75}\right)\right)\\
& +e^2\left(f^6\left(\frac{389C_{\mathrm{qv}}}{150}-\frac{389C_{\mathrm{qr}}}{450}\right)+f^4\left(-\frac{248C_{\mathrm{qr}}}{75}-\frac{389C_{\mathrm{qv}}}{150}\right)\right)\\
& +f^6\left(\frac{389C_{\mathrm{qr}}}{450}+\frac{1201C_{\mathrm{qv}}}{1800}\right)+\frac{142C_{\mathrm{qr}}e^8}{45}-\frac{1201C_{\mathrm{qv}}f^8}{1800}\\
\tilde{C}_{\mathrm{o10l}} & e^6\left(-\frac{71C_{\mathrm{ll}}}{45}+f^2\left(-\frac{71C_{\mathrm{lr}}}{15}-\frac{71C_{\mathrm{lv}}}{45}\right)-\frac{142C_{\mathrm{lr}}}{45}+\frac{71C_{\mathrm{lv}}}{45}\right)+e^4\left(f^2\left(\frac{107C_{\mathrm{ll}}}{75}+\frac{71C_{\mathrm{lr}}}{15}-\frac{248C_{\mathrm{lv}}}{75}\right)\right.\\
& \left.+f^4\left(\frac{248C_{\mathrm{lr}}}{75}+\frac{248C_{\mathrm{lv}}}{75}\right)\right)+e^2\left(f^4\left(-\frac{107C_{\mathrm{ll}}}{150}-\frac{248C_{\mathrm{lr}}}{75}+\frac{389C_{\mathrm{lv}}}{150}\right)+f^6\left(-\frac{389C_{\mathrm{lr}}}{450}-\frac{389C_{\mathrm{lv}}}{150}\right)\right)\\
& +f^6\left(\frac{71C_{\mathrm{ll}}}{360}+\frac{389C_{\mathrm{lr}}}{450}-\frac{1201C_{\mathrm{lv}}}{1800}\right)+\frac{142C_{\mathrm{lr}}e^8}{45}+\frac{1201C_{\mathrm{lv}}f^8}{1800}\\
\tilde{C}_{\mathrm{o12h}} & e^8\left(-\frac{59873C_{\mathrm{hl}}}{22500}+\frac{59873C_{\mathrm{hr}}}{11250}-\frac{59873C_{\mathrm{hv}}}{22500}\right)+e^6f^2\left(\frac{21989C_{\mathrm{hl}}}{5625}-\frac{59873C_{\mathrm{hr}}}{5625}+\frac{12628C_{\mathrm{hv}}}{1875}\right)\\
& +e^4f^4\left(-\frac{21989C_{\mathrm{hl}}}{7500}+\frac{6314C_{\mathrm{hr}}}{625}-\frac{53779C_{\mathrm{hv}}}{7500}\right)+e^2f^6\left(\frac{59873C_{\mathrm{hl}}}{45000}-\frac{53779C_{\mathrm{hr}}}{11250}+\frac{155243C_{\mathrm{hv}}}{45000}\right)\\
& +f^8\left(-\frac{91663C_{\mathrm{hl}}}{360000}+\frac{155243C_{\mathrm{hr}}}{180000}-\frac{72941C_{\mathrm{hv}}}{120000}\right)\\
\tilde{C}_{\mathrm{o12q}} & e^8\left(\frac{59873C_{\mathrm{qr}}}{11250}+\frac{59873C_{\mathrm{qv}}}{22500}\right)+e^6f^2\left(-\frac{59873C_{\mathrm{qr}}}{5625}-\frac{12628C_{\mathrm{qv}}}{1875}\right)+e^4f^4\left(\frac{6314C_{\mathrm{qr}}}{625}+\frac{53779C_{\mathrm{qv}}}{7500}\right)\\
& +e^2f^6\left(-\frac{53779C_{\mathrm{qr}}}{11250}-\frac{155243C_{\mathrm{qv}}}{45000}\right)+f^8\left(\frac{155243C_{\mathrm{qr}}}{180000}+\frac{72941C_{\mathrm{qv}}}{120000}\right)\\
\tilde{C}_{\mathrm{o12l}} & e^8\left(\frac{59873C_{\mathrm{ll}}}{22500}+\frac{59873C_{\mathrm{lr}}}{11250}-\frac{59873C_{\mathrm{lv}}}{22500}\right)+e^6f^2\left(-\frac{21989C_{\mathrm{ll}}}{5625}-\frac{59873C_{\mathrm{lr}}}{5625}+\frac{12628C_{\mathrm{lv}}}{1875}\right)\\
& +e^4f^4\left(\frac{21989C_{\mathrm{ll}}}{7500}+\frac{6314C_{\mathrm{lr}}}{625}-\frac{53779C_{\mathrm{lv}}}{7500}\right)+e^2f^6\left(-\frac{59873C_{\mathrm{ll}}}{45000}-\frac{53779C_{\mathrm{lr}}}{11250}+\frac{155243C_{\mathrm{lv}}}{45000}\right)\\
& +f^8\left(\frac{91663C_{\mathrm{ll}}}{360000}+\frac{155243C_{\mathrm{lr}}}{180000}-\frac{72941C_{\mathrm{lv}}}{120000}\right)
\end{array}
$$

Table A.1: Coefficients for auxiliary functions for analytical particle-core model.

$\tilde{C}_{\mathrm{o4c}}$	$\frac{f^2}{5} - \frac{2e^2}{5}$
$\tilde{C}_{\mathrm{o6c}}$	$\frac{2e^4}{7} - \frac{2e^2f^2}{7} + \frac{3f^4}{28}$
$\tilde{C}_{\mathrm{o8c}}$	$-\frac{196e^6}{675} + \frac{98e^4f^2}{225} - \frac{301e^2f^4}{900} + \frac{511f^6}{5400}$
$\tilde{C}_{\mathrm{o10c}}$	$\frac{71e^8}{180} - \frac{71e^6f^2}{90} + \frac{62e^4f^4}{75} - \frac{389e^2f^6}{900} + \frac{1201f^8}{14400}$
$\tilde{C}_{\mathrm{o2c}}$	$\frac{2}{3}$
$\tilde{C}_{\mathrm{o1c}}$	$-\frac{729e^8}{1600} + e^6\left(-\frac{81f^2}{400} - \frac{99}{200}\right) + e^4\left(-\frac{27f^4}{160} - \frac{39f^2}{200} - \frac{15}{28}\right)$
	$+e^2\left(-\frac{9f^6}{80} - \frac{33f^4}{200} - \frac{3f^2}{14} - \frac{3}{5}\right) - \frac{33f^8}{1600} - \frac{31f^6}{600} - \frac{3f^4}{28} - \frac{f^2}{5} - \frac{2}{3}$
$\tilde{C}_{\mathrm{il}}$	$e^8\left(\frac{18711C_{\mathrm{ll}}}{40000} - \frac{17253C_{\mathrm{lr}}}{40000} - \frac{18711C_{\mathrm{lv}}}{40000}\right) + f^8\left(\frac{1551C_{\mathrm{ll}}}{40000} - \frac{4653C_{\mathrm{lr}}}{40000} + \frac{3729C_{\mathrm{lv}}}{40000}\right)$
	$+e^6\left(f^2\left(-\frac{2673C_{\mathrm{ll}}}{10000} - \frac{6561C_{\mathrm{lr}}}{10000} - \frac{2187C_{\mathrm{lv}}}{10000}\right) + \frac{81C_{\mathrm{ll}}}{200} - \frac{27C_{\mathrm{lr}}}{40} - \frac{81C_{\mathrm{lv}}}{200}\right)$
	$+e^4\left(f^4\left(\frac{297C_{\mathrm{ll}}}{20000} - \frac{5211C_{\mathrm{lr}}}{20000} - \frac{4617C_{\mathrm{lv}}}{20000}\right) + f^2\left(-\frac{27C_{\mathrm{ll}}}{200} - \frac{87C_{\mathrm{lr}}}{200} - \frac{57C_{\mathrm{lv}}}{200}\right)\right.$
	$\left.+\frac{39C_{\mathrm{ll}}}{100} - \frac{579C_{\mathrm{lr}}}{700} - \frac{39C_{\mathrm{lv}}}{100}\right) + \frac{2C_{\mathrm{ll}}}{5} - \frac{6C_{\mathrm{lr}}}{5} - \frac{2C_{\mathrm{lv}}}{5}$
	$+e^2\left(f^6\left(\frac{1683C_{\mathrm{ll}}}{10000} - \frac{3789C_{\mathrm{lr}}}{10000} + \frac{2097C_{\mathrm{lv}}}{10000}\right) + f^4\left(\frac{27C_{\mathrm{ll}}}{200} - \frac{69C_{\mathrm{lr}}}{200} - \frac{3C_{\mathrm{lv}}}{200}\right)\right.$
	$+f^2\left(\frac{3C_{\mathrm{ll}}}{50} - \frac{123C_{\mathrm{lr}}}{350} - \frac{81C_{\mathrm{lv}}}{350}\right) + \frac{3C_{\mathrm{ll}}}{7} - \frac{33C_{\mathrm{lr}}}{35} - \frac{3C_{\mathrm{lv}}}{7}\Big) + f^6\left(\frac{3C_{\mathrm{ll}}}{40} - \frac{9C_{\mathrm{lr}}}{40} + \frac{29C_{\mathrm{lv}}}{200}\right)$
	$+f^4\left(\frac{11C_{\mathrm{ll}}}{100} - \frac{33C_{\mathrm{lr}}}{100} + \frac{83C_{\mathrm{lv}}}{700}\right) + f^2\left(\frac{C_{\mathrm{ll}}}{7} - \frac{3C_{\mathrm{lr}}}{7} - \frac{C_{\mathrm{lv}}}{35}\right)$
$\tilde{C}_{\mathrm{ih}}$	$e^8\left(-\frac{18711C_{\mathrm{hl}}}{40000} - \frac{17253C_{\mathrm{hr}}}{40000} - \frac{18711C_{\mathrm{hv}}}{40000}\right) + f^8\left(-\frac{1551C_{\mathrm{hl}}}{40000} - \frac{4653C_{\mathrm{hr}}}{40000} + \frac{3729C_{\mathrm{hv}}}{40000}\right)$
	$+e^6\left(f^2\left(\frac{2673C_{\mathrm{hl}}}{10000} - \frac{6561C_{\mathrm{hr}}}{10000} - \frac{2187C_{\mathrm{hv}}}{10000}\right) - \frac{81C_{\mathrm{hl}}}{200} - \frac{27C_{\mathrm{hr}}}{40} - \frac{81C_{\mathrm{hv}}}{200}\right)$
	$+f^2\left(-\frac{C_{\mathrm{hl}}}{7} - \frac{3C_{\mathrm{hr}}}{7} - \frac{C_{\mathrm{hv}}}{35}\right) + f^6\left(-\frac{3C_{\mathrm{hl}}}{40} - \frac{9C_{\mathrm{hr}}}{40} + \frac{29C_{\mathrm{hv}}}{200}\right)$
	$+e^4\left(f^4\left(-\frac{297C_{\mathrm{hl}}}{20000} - \frac{5211C_{\mathrm{hr}}}{20000} - \frac{4617C_{\mathrm{hv}}}{20000}\right) + f^2\left(\frac{27C_{\mathrm{hl}}}{200} - \frac{87C_{\mathrm{hr}}}{200} - \frac{57C_{\mathrm{hv}}}{200}\right)\right.$
	$\left.-\frac{39C_{\mathrm{hl}}}{100} - \frac{579C_{\mathrm{hr}}}{700} - \frac{39C_{\mathrm{hv}}}{100}\right) + e^2\left(f^6\left(-\frac{1683C_{\mathrm{hl}}}{10000} - \frac{3789C_{\mathrm{hr}}}{10000} + \frac{2097C_{\mathrm{hv}}}{10000}\right)\right.$
	$+f^4\left(-\frac{27C_{\mathrm{hl}}}{200} - \frac{69C_{\mathrm{hr}}}{200} - \frac{3C_{\mathrm{hv}}}{200}\right) + f^2\left(-\frac{3C_{\mathrm{hl}}}{50} - \frac{123C_{\mathrm{hr}}}{350} - \frac{81C_{\mathrm{hv}}}{350}\right) - \frac{3C_{\mathrm{hl}}}{7} - \frac{33C_{\mathrm{hr}}}{35} - \frac{3C_{\mathrm{hv}}}{7}\Big)$
	$+f^4\left(-\frac{11C_{\mathrm{hl}}}{100} - \frac{33C_{\mathrm{hr}}}{100} + \frac{83C_{\mathrm{hv}}}{700}\right) - \frac{2C_{\mathrm{hl}}}{5} - \frac{6C_{\mathrm{hr}}}{5} - \frac{2C_{\mathrm{hv}}}{5}$
$\tilde{C}_{\mathrm{iq}}$	$e^8\left(\frac{18711C_{\mathrm{qv}}}{40000} - \frac{17253C_{\mathrm{qr}}}{40000}\right) + e^6\left(f^2\left(\frac{2187C_{\mathrm{qv}}}{10000} - \frac{6561C_{\mathrm{qr}}}{10000}\right) - \frac{27C_{\mathrm{qr}}}{40} + \frac{81C_{\mathrm{qv}}}{200}\right)$
	$+e^4\left(f^4\left(\frac{4617C_{\mathrm{qv}}}{20000} - \frac{5211C_{\mathrm{qr}}}{20000}\right) + f^2\left(\frac{57C_{\mathrm{qv}}}{200} - \frac{87C_{\mathrm{qr}}}{200}\right) - \frac{579C_{\mathrm{qr}}}{700} + \frac{39C_{\mathrm{qv}}}{100}\right)$
	$+e^2\left(f^6\left(-\frac{3789C_{\mathrm{qr}}}{10000} - \frac{2097C_{\mathrm{qv}}}{10000}\right) + f^4\left(\frac{3C_{\mathrm{qv}}}{200} - \frac{69C_{\mathrm{qr}}}{200}\right) + f^2\left(\frac{81C_{\mathrm{qv}}}{350} - \frac{123C_{\mathrm{qr}}}{350}\right)\right.$
	$\left.-\frac{33C_{\mathrm{qr}}}{35} + \frac{3C_{\mathrm{qv}}}{7}\right) + f^8\left(-\frac{4653C_{\mathrm{qr}}}{40000} - \frac{3729C_{\mathrm{qv}}}{40000}\right) + f^6\left(-\frac{9C_{\mathrm{qr}}}{40} - \frac{29C_{\mathrm{qv}}}{200}\right)$
	$+f^4\left(-\frac{33C_{\mathrm{qr}}}{100} - \frac{83C_{\mathrm{qv}}}{700}\right) + f^2\left(\frac{C_{\mathrm{qv}}}{35} - \frac{3C_{\mathrm{qr}}}{7}\right) - \frac{6C_{\mathrm{qr}}}{5} + \frac{2C_{\mathrm{qv}}}{5}$

Table A.2: Coefficients for auxiliary functions for analytical particle-core model (continued).

B Test accelerator parameters

TEST1			
Parameter	Value	Unit	Description
a_x	4.7	mm	initial radial core semi-axis
a_y	3.6	mm	initial vertical core semi-axis
a_z	5.2	mm	initial longitudinal core semi-axis
f_{RF}	50.637	MHz	RF frequency
h	10	-	harmonic number
f_{rev}	5.0637	MHz	revolution frequency of particles
I	2.4	mA	current (mean)
κ	$2.02 \cdot 10^{-6}$	-	generalized perveance
E	29.7	MeV	kinetic energy
ν_r	1.306	-	radial tune
ν_y	1.683	-	vertical tune
ν_l	0.75	-	longitudinal tune*

corresponds to an Injector 2 like machine for a coasting beam in turn 40.
*) in longitudinal direction no data has been available and the focusing is therefore approximated as linear focusing with a focusing constant that compensates the bunch spread due to space charge.

Table B.1: Parameters for test accelerator TEST1 (coasting beam).

TEST2			
Parameter	Value	Unit	Description
a_x	4.7	mm	radial core semi-axis
a_y	2.5	mm	vertical core semi-axis
a_z	6.8	mm	longitudinal core semi-axis
f_{RF}	50.637	MHz	RF frequency
h	10	-	harmonic number
f_{rev}	5.0637	MHz	revolution frequency of particles
I	2.4	mA	current (mean)
κ	$4.52 \cdot 10^{-5} - 7.80 \cdot 10^{-7}$	-	generalized perveance
E	$1.38 - 72$	MeV	kinetic energy
ν_r	$1.20 - 1.35$	-	radial tune
ν_y	$1.35 - 1.68$	-	vertical tune
ν_l	0.8	-	longitudinal tune*
radius	48 - 312	cm	orbit radius

*) in longitudinal direction no data has been available and the focusing is therefore approximated as linear focusing with a focusing constant that compensates the bunch spread due to space charge.

Table B.2: Parameters for test accelerator TEST2.

TEST3			
Parameter	Value	Unit	Description
a_x	4.7	mm	radial core semi-axis
a_y	2.5	mm	vertical core semi-axis
a_z	6.8	mm	longitudinal core semi-axis
f_{rev}	5.0637	MHz	revolution frequency of particles
I	2.4	mA	current (mean)
κ	$4.52 \cdot 10^{-5} - 7.80 \cdot 10^{-7}$	-	generalized perveance
E	$1.38 - 72$	MeV	kinetic energy
ν_r	$1.20 - 1.35$	-	radial tune
ν_y	$1.35 - 1.68$	-	vertical tune
ν_l	0.55	-	longitudinal tune*
radius	48 - 312	cm	orbit radius

*) in longitudinal direction no data has been available and the focusing is therefore approximated as linear focusing with a focusing constant that compensates the bunch spread due to space charge.

Table B.3: Parameters for test accelerator TEST3.

C Lists

C.1 List of Figures

C.2 List of Tables

D Listings

E Bibliography

[1] R. L. Gluckstern. Analytic model for halo formation in high current ion linacs. *Physical Review Letters*, 73(9):1247–1250, 1994.

[2] J.J. Yang, A. Adelmann, M. Humbel, M. Seidel, and T.J. Zhang. Beam dynamics in high intensity cyclotrons including neighboring bunch effects: Model, implementation, and application. *Physical Review Special Topics - Accelerators and Beams*, 13(6), 2010.

[3] Y.J. Bi, A. Adelmann, R. Dölling, M. Humbel, W. Joho, M. Seidel, and T.J. Zhang. Towards quantitative simulations of high power proton cyclotrons. *Physical Review Special Topics - Accelerators and Beams*, 14(5), 2011.

[4] M. Ikegami, S. Machida, and T. Uesugi. Particle-core analysis of dispersion effects on beam halo formation. *Physical Review Special Topics - Accelerators and Beams*, 2(12):46–55, 1999.

[5] S. M. Lund and J. J. Barnard. Theory of longitudinal beam halo in rf linacs II: Envelope-particle resonances. In *Particle Accelerator Conference, 1997. Proceedings of the 1997*, volume 2, pages 1932–1934 vol.2, 1997.

[6] M. Ikegami. Particle-core analysis of mismatched beams in a periodic focusing channel. *Physical Review E - Statistical Physics, Plasmas, Fluids, and Related Interdisciplinary Topics*, 59 (2 PART B):2330–2338, 1999.

[7] A. Riabko, M. Ellison, X. Kang, S. Y. Lee, D. Li, J. Y. Liu, X. Pei, and L. Wang. Hamiltonian formalism for space charge dominated beams in a uniform focusing channel. *Physical Review E*, 51(4):3529–3546, 1995.

[8] J. D. Lawson. Perveance and the bennett pinch relation in partially-neutralized electron beams. *Journal of Electronics and Control*, 5(2):146–151, 1958.

[9] Oliver Dimon Kellogg. *Foundations of potential theory*. Springer, Berlin, 1967.

[10] M Pabst, K Bongardt, and A Letchford. Progress on intense proton beam dynamics and halo formation.

[11] B. C. Carlson. Elliptic integrals: Symmetric integrals. In *NIST Digital Library of Mathematical Functions*. National Institute of Standards and Technology, 2010.

[12] W. J. G. M. Kleeven. *Theory of Accelerated Orbits and Space Charge Effects in an AVF Cyclotron*. Technische Universiteit Eindhoven, Eindhoven, 1988.